

# Stability and Intervehicle Distance Analysis of Vehicular Platoons: Highlighting the Impact of Bidirectional Communication Topologies

Amir Zakerimanesh<sup>1</sup>, *Graduate Student Member, IEEE*, Tony Z. Qiu<sup>2</sup>, *Member, IEEE*, Mahdi Tavakoli<sup>1</sup>, *Senior Member, IEEE*

**Abstract**—Vehicular platooning, a configuration comprising a leading vehicle and multiple follower vehicles (FVs) seeks to achieve and maintain specific intervehicle distances (IDs) while synchronizing FVs with the velocity and acceleration of the leading vehicle. Prior to attaining a desired stable state, the IDs may undergo transient fluctuations. While the attainment of internal stability is pivotal for realizing the intended spacing between vehicles, it does not inherently guarantee that these transient fluctuations remain within safe thresholds, thereby mitigating the risk of collisions. Communication between vehicles has a critical role in vehicular platooning and significantly influences these transient distance fluctuations. Consequently, we present a mapping between the initial conditions and these transient fluctuations which hinges on the communication topology, as well as the control parameters. Specifically, our focus is directed towards bidirectional communication topologies (BDCTs), wherein FVs possess the capability to communicate both with preceding and subsequent vehicles within the platoon. Investigation of these mappings illuminates the advantages and disadvantages of various BDCTs. Notably, we discern that within BDCTs, the receipt of information from a greater number of vehicles situated behind may at times hinder the overall performance of the platoon, resulting in larger deviations from the desired intervehicle distances or the velocity and acceleration of the leading vehicle. In contrast, information derived from vehicles located ahead, particularly the leading vehicle itself, serves to enhance intervehicle distances and thereby contributes significantly to the safety of the platoon. In conclusion, our theoretical insights are substantiated through a series of simulations.

**Index Terms**—Platoon, Stability, Transient Behavior, Formation Control, Bidirectional Communications

## I. INTRODUCTION

A group of vehicles, led by one primary vehicle and followed by several others, forms what is known as a vehicular platoon. The primary objective of platooning is twofold: firstly, to attain and maintain the desired intervehicle distances (IDs), and secondly, to ensure that the follower vehicles (FVs) closely mirror the speed and acceleration of the lead vehicle. This collaborative formation brings several advantages. Firstly, due to the reduced space between vehicles, there is

a significant decrease in aerodynamic drag between them, resulting in a substantial reduction in fuel consumption [1], [2]. Furthermore, the tight spacing of vehicles in a platoon allows for the accommodation of more vehicles on the road, thus enhancing highway capacity. Additionally, platooning systems are designed to enable automated and rapid responses by follower vehicles to the lead vehicle's actions, thereby contributing to the overall safety of drivers [3], [4]. To achieve these objectives, various spacing policies have been utilized, including constant time headway [5], nonlinear [6], delay-based [7], and constant distance [8], [9] policies. This work focuses on the constant distance policy, which seeks to establish and sustain fixed distances between adjacent vehicles. Platoon dynamics encompass considerations of vehicle dynamics, communication topology (CT), distributed controllers, and spacing policies [10], [11]. In this study, the emphasis is placed on the longitudinal motion of vehicles and the utilization of distributed linear controllers [12], [13], [14].

Communication topology, which governs how vehicles exchange essential information such as position, velocity, and acceleration, holds a central position in determining platoon stability and performance. While existing literature extensively examines the stability and performance of vehicle platoons within specific CTs, there is a limited focus on differentiating the impact of CTs on platoon performance. Recent studies have started addressing this gap. In [15], a general graph theory framework is applied to explore the impact of connectivity measures within CTs on the performance of distributed algorithms. This investigation assesses the ability of these algorithms to mitigate communication disruptions, detect cyber-attacks, and uphold resilience against such challenges. Additionally, [16] delves into the distinctions among three unidirectional communication topologies (UCTs) and their implications on stability, robustness, safety, and emissions within vehicle platoons. In terms of safety analysis, this study relies on two metrics, maximum time to collision (MTTC) and deceleration rate to avoid a crash (DRAC), to assess and contrast the security performance of platoons operating under the influence of three different UCTs. It is worth mentioning that in UCTs, vehicles only receive data from vehicles ahead of them. On the other hand, one aspect of platooning that has received limited attention in the existing literature is the transient behavior of IDs, a critical factor closely linked to platoon safety. It is worth noting that favorable transient behaviors, as well as steady-state conditions, as studied in

This research is supported by the Government of Alberta's grant to Centre for Autonomous Systems in Strengthening Future Communities (RCP-19-001-MIF).

<sup>1</sup>A. Zakerimanesh, and M. Tavakoli are with the Department of Electrical and Computer Engineering, University of Alberta, Edmonton T6G 1H9, Alberta, Canada. {amir.zakerimanesh, mahdi.tavakoli}@ualberta.ca

<sup>2</sup>T. Z. Qiu is with Department of Civil and Environmental Engineering, University of Alberta, Edmonton, Canada. {tony.qiu}@ualberta.ca

[17], can significantly contribute to preventing intervehicular collisions and enhancing the overall safety of platooning.

Therefore, in addition to the roles of controllers, vehicle features, and initial conditions, communication structures play a pivotal role in influencing platooning dynamics, particularly their impact on transient distances between vehicles. This study thoroughly explores this critical aspect by focusing on transient intervehicle distance errors (TIDEs). In our definition, TIDEs quantify momentary deviations in spacing between neighboring vehicles before their distances align with the intended values. Our specific investigation centers on how various bidirectional communication topologies (BDCTs) affect TIDEs, as these transient distances are paramount in determining the safety and collision-free operation of platoons. Notably, unlike unidirectional communication topologies (UCTs), BDCTs enable vehicles following one another to exchange their current state information with both preceding and succeeding vehicles. This paper's contributions can be summarized as follows:

- 1) **Novel Dynamic Model:** We have introduced a novel closed-loop dynamic model for vehicular platoons, shifting our focus from differences between follower-leader states to differences among neighboring vehicles. This approach allows for the relaxation of the requirement for the leader vehicle's velocity to remain constant for intervehicle distance convergence of FVs and for followers to reach their desired velocities and accelerations. As a result, the key determinant for the convergence lies solely in achieving internal stability.
- 2) **Analysis of Transient Interverhicle Distances:** Our findings indicate that the deviation levels of transient intervehicle distances from their desired values are depend on crucial parameters such as the leader vehicle's acceleration, initial conditions, control gains, the engine time constants of follower vehicles (FVs), the number of FVs in the platoon, and the communication type employed.
- 3) **Analytical Distance Trajectories:** We have developed analytical distance trajectories for each pair of neighboring vehicles, revealing their behavior across different bidirectional communication topologies (BDCTs).
- 4) **Communication Topology Insights 1:** We have highlighted the advantages and disadvantages of various BDCTs. Our observations suggest that, within the domain of distributed controllers, the collection of data from a greater number of vehicles ahead, especially the leading vehicle, has the potential to reduce the likelihood of breaching safe intervehicle distances in BDCTs. Although our focus differs from the study in [16], our findings align with their conclusion, emphasizing that predecessor-leader-following (PLF) and multiple-predecessor-leader-following (MPLF) configurations are notably superior to predecessor-following (PF).
- 5) **Communication Topology Insights 2:** Conversely, incorporating information from more vehicles behind can have an adverse impact on intervehicle distances, elevating the risk of breaching the safe spacing between vehicles.

- 6) **Enhanced Platoon Performance:** We have demonstrated that broadcasting the leader vehicle's state to other vehicles has the potential to improve overall platoon performance. This leads to smaller deviations from desired values during transient states.
- 7) **Simulation Validation:** We have provided simulations to validate our theoretical findings and support our research contributions.

In summary, our work emphasizes the importance of studying transient intervehicle distances and their relationship with various bidirectional communication topologies.

## II. NOMENCLATURE

In this paper, the time argument of signals will only be included if they enhance clarity. To differentiate between elements within vertical and horizontal vectors, we will utilize the semicolon and colon symbols, respectively. For instance, a 3-by-1 vector is symbolized as  $[\cdot; \cdot; \cdot]$ , while a 1-by-3 vector takes the form of  $[\cdot, \cdot, \cdot]$ . This notation will be consistently employed throughout the document to improve lucidity and ease of reading. The following section provides an overview of the important parameters and variables utilized in this paper:

$n$	Number of follower vehicles
$s$	Laplace variable
ID	Interverhicle distance
TID	Transient intervehicle distance
TIDE	Transient intervehicle distance error
BDCTs	Bidirectional communication topologies
FV	Follower vehicle
BDL	Bidirectional-leader
BD	Bidirectional
TBPF	Two-bidirectional-predecessor-following
TPSF	Two-predecessor-single-following
SPTF	Single-predecessor-two-following
$x_{i+1}$	Position of the $(i+1)^{th}$ vehicle
$\Delta x_{i+1}^j$	$x_{i+1} - x_j$
$\dot{x}_{i+1}$	Velocity ( $v_{i+1}$ ) of the $(i+1)^{th}$ vehicle
$\Delta \dot{x}_{i+1}^j$	$\dot{x}_{i+1} - \dot{x}_j$
$\ddot{x}_{i+1}$	Acceleration ( $a_{i+1}$ ) of the $(i+1)^{th}$ vehicle
$\Delta \ddot{x}_{i+1}^j$	$\ddot{x}_{i+1} - \ddot{x}_j$
$\ddot{\ddot{x}}_{i+1}$	Jerk ( $\mathcal{J}_{i+1}$ ) of the $(i+1)^{th}$ vehicle
$\Delta \ddot{\ddot{x}}_{i+1}^j$	$\ddot{\ddot{x}}_{i+1} - \ddot{\ddot{x}}_j$
$\mathbf{X}_{i+1}$	$[x_{i+1}; \dot{x}_{i+1}; \ddot{x}_{i+1}]$
$\dot{\mathbf{X}}_{i+1}$	$[\dot{x}_{i+1}; \ddot{x}_{i+1}; \ddot{\ddot{x}}_{i+1}]$
$x_{i+1}^*$	Desired position of the $(i+1)^{th}$ vehicle
$\dot{x}_{i+1}^*$	Desired velocity of the $(i+1)^{th}$ vehicle
$\ddot{x}_{i+1}^*$	Desired acceleration of the $(i+1)^{th}$ vehicle
$\hat{x}_{i+1}$	$x_{i+1} - x_{i+1}^*$
$\Delta \hat{p}_i^{i+1}$	$\hat{x}_i - \hat{x}_{i+1}$
$\mu$	$\Delta \hat{p}_i^{i+1}(0)$
$\dot{\hat{x}}_{i+1}$	$\dot{x}_{i+1} - \dot{x}_{i+1}^*$
$\Delta \hat{v}_i^{i+1}$	$\hat{x}_i - \hat{x}_{i+1}$
$\ddot{\hat{x}}_{i+1}$	$\ddot{x}_{i+1} - \ddot{x}_{i+1}^*$
$\Delta \hat{a}_i^{i+1}$	$\hat{x}_i - \hat{x}_{i+1}$
$\ddot{\ddot{\hat{x}}}_{i+1}$	$\ddot{\ddot{x}}_{i+1} - \ddot{\ddot{x}}_{i+1}^*$
$\Delta \hat{\mathcal{J}}_i^{i+1}$	$\ddot{\ddot{x}}_i - \ddot{\ddot{x}}_{i+1}$

$\tilde{\mathbf{X}}_{i+1}^{i+1}$	$[\tilde{x}_{i+1}; \dot{\tilde{x}}_{i+1}; \ddot{\tilde{x}}_{i+1}]$
$\Delta\tilde{\mathbf{X}}_i^{i+1}$	$[\Delta\tilde{p}_i^{i+1}; \Delta\tilde{v}_i^{i+1}; \Delta\tilde{a}_i^{i+1}]$
$\Delta\tilde{\mathbf{X}}_i^{i+1}$	$[\Delta\tilde{v}_i^{i+1}; \Delta\tilde{a}_i^{i+1}; \Delta\tilde{j}_i^{i+1}]$
$\tilde{\mathbf{X}}_t$	$[\tilde{\mathbf{X}}_1; \tilde{\mathbf{X}}_2; \dots; \tilde{\mathbf{X}}_n]$
$\Delta\tilde{\mathbf{X}}_t$	$[\Delta\tilde{\mathbf{X}}_0^1; \Delta\tilde{\mathbf{X}}_1^2; \dots; \Delta\tilde{\mathbf{X}}_{n-1}^n]$
$\tau$	Engine time-constant of vehicles
$d_i^{i+1}$	Desired distance between vehicles $i$ and $i+1$
$D_i^{i+1}$	Distance between vehicles $i$ and $i+1$
$L_i$	Length of the $i^{\text{th}}$ vehicle
$\omega_i^{i+1}$	$L_i + d_i^{i+1}$
$d_{i+1,j}$	Desired position difference between vehicles $i+1$ and $j$
$k$	Coefficient of position errors in the distributed controller
$b$	Coefficient of velocity errors in the distributed controller
$h$	Coefficient of acceleration errors in the distributed controller
$\mathbf{K}$	$[k, b, h]$
$z_{i+1}^i=1$	Indicates vehicle $i+1$ receives information from vehicle $i$
$z_{i+1}^i=0$	Indicates vehicle $i+1$ does not receive information from vehicle $i$
$\mathbb{I}_{i+1}$	Set of vehicles from which the $(i+1)^{\text{th}}$ follower gets information
$\mathbb{R}_{i+1}$	$=\mathbb{I}_{i+1} - \{i\}$
$\mathbb{R}_i$	$=\mathbb{I}_i - \{i+1\}$
$\alpha_i$	Vehicles ahead providing info only to $i^{\text{th}}$ follower in pair $(i, i+1)$
$\beta_i$	Vehicles behind providing info only to $(i+1)^{\text{th}}$ follower in pair $(i, i+1)$
$\mathbf{M}_i$	Vehicles ahead ( $j \leq i$ ) providing info to $(i+1)^{\text{th}}$ follower in pair $(i, i+1)$
$\mathbf{B}_i$	Vehicles behind ( $j \geq i+1$ ) providing info to $i^{\text{th}}$ follower in pair $(i, i+1)$
$\mathbf{J}_i$	Union of $\mathbf{M}_i$ and $\mathbf{B}_i$
$ \cdot $	Cardinality of a set
$\mathbf{k}_{i+1}$	$=  \mathbb{I}_{i+1} k$
$\mathbf{b}_{i+1}$	$=  \mathbb{I}_{i+1} b$
$\mathbf{h}_{i+1}$	$= 1 +  \mathbb{I}_{i+1} h$
$\mathbb{K}_{i+1}$	$= [\mathbf{k}_{i+1}, \mathbf{b}_{i+1}, \mathbf{h}_{i+1}]$
$\mathbb{K}$	$= [k, b, 1+h]$
$\bar{k}_i$	$= \frac{ \mathbf{J}_i k}{\tau}$
$\bar{b}_i$	$= \frac{ \mathbf{J}_i b}{\tau}$
$\bar{h}_i$	$= \frac{1 +  \mathbf{J}_i h}{\tau}$
$\epsilon_{i+1}$	$= -\frac{\tau}{\tau} a_0 - \dot{a}_0$ , $a_0$ is leader acceleration
$\epsilon_{i+1}$	$= [0; 0; \epsilon_{i+1}]$
$\mathbf{Vec}(\cdot)$	Concatenates its arguments vertically
$\tilde{\mathbf{A}}_t$	Closed-loop system matrix with $\tilde{\mathbf{X}}_t$ as the platoon's total state vector
$\tilde{\mathbf{A}}_{\Delta t}$	Closed-loop system matrix with $\Delta\tilde{\mathbf{X}}_t$ as the platoon's total state vector
$\mathbf{A}_i^{i+1}$	System matrix for coupled dynamics of neighboring vehicles
$\Delta\tilde{p}_{i,zi}^{i+1}$	TIDE of neighboring vehicles $i$ and $i+1$ excited by the pair's initial condition (zero input)
$\Delta\tilde{p}_{i,zs}^{i+1}$	TIDE of neighboring vehicles $i$ and $i+1$ when

$\Delta\tilde{p}_i^{i+1}(0)=0$	(zero state)
$\Delta\tilde{\mathbf{P}}$	$= [\Delta\tilde{p}_0^1; \Delta\tilde{p}_1^2; \dots; \Delta\tilde{p}_{n-1}^n]$
$U(\cdot)$	The unit step function
$\mu$	Initial IDE between adjacent vehicles
$\Delta\tilde{u}_i^{i+1}$	Input signal for coupled dynamics of neighboring vehicles $i$ and $i+1$
$\Psi_i$	TIDE of neighboring vehicles $i$ and $i+1$ excited by all relevant initial conditions
$\Psi$	$[\Psi_0; \Psi_1; \dots; \Psi_{n-1}]$
$\mathbf{Q}$	Matrix mapping initial conditions to TIDEs
$d_{i,i+1}^s$	Safe distance between neighboring vehicles

### III. PRELIMINARIES

#### A. Bidirectional Communication Topologies (BDCTs)

Fig. 1 displays common BDCTs employed in vehicle platooning. In this context, each follower vehicle (FV) possesses the ability to communicate its state, including position, velocity, and acceleration, with both the vehicles ahead and those behind. This interplay establishes a bidirectional flow of communication across all vehicles. Subsequently, to maintain conciseness, unless specifically stated otherwise, we will collectively denote the state information of each vehicle, comprising its position, velocity, and acceleration, as simply ‘information’.

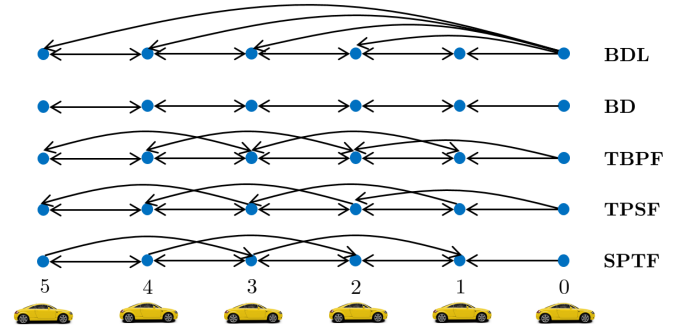


Fig. 1: Exemplification of different common BDCTs between vehicles. The leading vehicle (referred to as the leader) is designated as 0, while the FVs are labeled from 1 to 5.

In the depicted bidirectional-leader (BDL) topology in Fig. 1, each FV receives information from the leader vehicle. Simultaneously, every FV exchanges information with both its immediate succeeding and preceding vehicles. Similarly, within the bidirectional (BD) topology, each FV participates in information exchange with both its following and preceding vehicles. In the two-bidirectional-predecessor-following (TBPF) topology, each FV communicates with its two immediate followers and two immediate predecessors. In the two-predecessor-single-following (TPSF) topology, each follower vehicle (FV) obtains information from its two immediate predecessors and one immediate follower. Also, each FV conveys its own state to its two immediate followers and one immediate preceding vehicle. In the single-predecessor-two-following (SPTF) topology, each FV acquires information from its two immediate followers and one immediate predecessor. Furthermore, each FV sends its state to its two immediate predecessors and one immediate following vehicles.

Consider the platoon shown in Fig. 1 and, in preparation for later use, let for the pairwise vehicles  $(i, i+1)$  where  $i$  ranges from 0 to  $n-1$  (with  $n=5$  for the showcased platoon), the following sets be defined as:

- 1)  $\mathbb{I}_{i+1}$ : Vehicles from which the  $(i+1)^{th}$  follower gets information. For example, in TPSF topology for pair (2,3),  $\mathbb{I}_3$  is  $\{1,2,4\}$ .
- 2)  $\mathbb{I}_i$ : Vehicles from which the  $i^{th}$  follower obtains information. In TPSF topology for pair (2,3),  $\mathbb{I}_2$  is  $\{0,1,3\}$ .
- 3)  $\mathbb{R}_{i+1}$ : Vehicles, excluding vehicle  $i$ , providing information to the  $(i+1)^{th}$  follower. In SPTF topology for pair (2,3),  $\mathbb{R}_3$  is  $\{4,5\}$ .
- 4)  $\mathbb{R}_i$ : Vehicles, excluding vehicle  $i+1$ , supplying information to the  $i^{th}$  follower. In SPTF topology for pair (2,3),  $\mathbb{R}_2$  is  $\{1,4\}$ .

We also use  $z_i^j$  to represent the information linkage between vehicles  $i$  and  $j$ , where  $z_i^j=1$  means vehicle  $i$  gets information from vehicle  $j$ , and  $z_i^j=0$  means it does not. For TPSF topology, examples are  $z_3^1=1$  and  $z_4^1=0$  (Figure 1).

### B. Representation of Constant and Changing Distances

We use a left-to-right direction for vehicle movement, designated as  $\rightarrow$  for positive direction, and  $\leftarrow$  for negative direction. Constant lengths or distances are represented by  $\leftrightarrow$ . In Figure 2,  $L_i$  and  $L_{i+1}$  indicate vehicle lengths, while  $d_i^{i+1}$  represents the desired constant gap between them. For instance, arbitrary variable distances  $s_1, s_2, s_3$ , and  $s_4$  follow the formulas:  $s_1=x_i-x_{i+1}$ ,  $s_2=x_{i+1}-(x_i-L_i)$ ,  $s_3=x_{i+1}$ , and  $s_4=x_i$ . Here,  $x_i$  and  $x_{i+1}$  refer to the front-side positions of the vehicles.

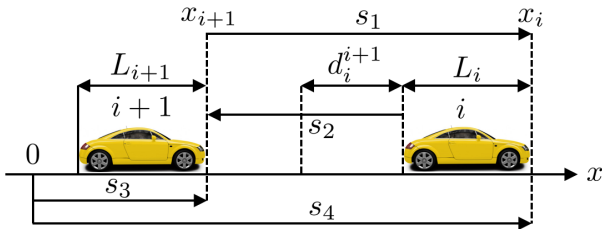


Fig. 2: Illustrating adjacent vehicles: Vehicle  $i+1$  as the follower and vehicle  $i$  as the predecessor, showing constant and changing distances.

### C. Vehicles Dynamics and 'Follower-Leader' State Errors

We make the assumption that the leading vehicle does not undergo any control process. Instead, the position, velocity, and acceleration of the leading vehicle are utilized to govern the behavior of the subsequent vehicles. In this context, each following vehicle's behavior within the platoon is described mathematically using a third-order linear model [18], [12], [14], [19], [20], [21], [22], [23], [24], [25]. This model is defined as:

$$\begin{cases} \dot{x}_{i+1}=v_{i+1} \\ \dot{v}_{i+1}=a_{i+1} \\ \dot{a}_{i+1}=-\frac{1}{\tau}a_{i+1}+\frac{1}{\tau}u_{i+1} \end{cases} \quad i=0, \dots, n-1 \quad (1)$$

Here,  $a_{i+1}$ ,  $v_{i+1}$ , and  $\tau$  represent the acceleration, velocity, and engine time constant of the  $(i+1)^{th}$  follower. Let  $\mathbf{X}_{i+1} \triangleq [x_{i+1}; \dot{x}_{i+1}; \ddot{x}_{i+1}]$  define the state vector of the  $(i+1)^{th}$  follower, where  $\dot{x}_{i+1}=v_{i+1}$  and  $\ddot{x}_{i+1}=a_{i+1}$ . Consequently, for  $i=0, \dots, n-1$ , and given the equation (1), the state-space model for the  $(i+1)^{th}$  follower can be represented as:

$$\dot{\mathbf{X}}_{i+1} = \underbrace{\begin{bmatrix} 0 & 1 & 0 \\ 0 & 0 & 1 \\ 0 & 0 & -\frac{1}{\tau} \end{bmatrix}}_{\triangleq \mathbf{A}} \mathbf{X}_{i+1} + \underbrace{\begin{bmatrix} 0 \\ 0 \\ \frac{1}{\tau} \end{bmatrix}}_{\triangleq \mathbf{B}} u_{i+1} \quad (2)$$

The controller  $u_{i+1}$  will be discussed subsequently. For each index  $i=0, \dots, n-1$ , the desired position denoted as  $x_{i+1}^*$ , desired velocity denoted as  $\dot{x}_{i+1}^*$ , and desired acceleration denoted as  $\ddot{x}_{i+1}^*$  of the  $(i+1)^{th}$  follower with respect to the state of the leader vehicle are defined as follows:

$$x_{i+1}^* \triangleq x_0 - \sum_{\kappa=0}^i (L_{\kappa} + d_{\kappa}^{\kappa+1}), \quad \dot{x}_{i+1}^* = v_0, \quad \text{and} \quad \ddot{x}_{i+1}^* = a_0 \quad (3)$$

regarding which let the desired state vector of the  $(i+1)^{th}$  follower be denoted as  $\mathbf{X}_{i+1}^* \triangleq [x_{i+1}^*; \dot{x}_{i+1}^*; \ddot{x}_{i+1}^*]$ . It is important to observe that our specified reference values in (3) are in contrast to those presented in [18], [12], [14], where  $\ddot{x}_{i+1}^*$  was set to 0. Through these considerations, the desired state of the followers are calculated with respect to the state of the leader vehicle. Therefore, let 'follower-leader' state error of the  $(i+1)^{th}$  follower be defined as  $\tilde{\mathbf{X}}_{i+1} \triangleq \mathbf{X}_{i+1} - \mathbf{X}_{i+1}^* = [\tilde{x}_{i+1}; \tilde{\dot{x}}_{i+1}; \tilde{\ddot{x}}_{i+1}]$  where  $\tilde{x}_{i+1} = x_{i+1} - x_{i+1}^*$ ,  $\tilde{\dot{x}}_{i+1} = \dot{x}_{i+1} - \dot{x}_{i+1}^*$ , and  $\tilde{\ddot{x}}_{i+1} = \ddot{x}_{i+1} - \ddot{x}_{i+1}^*$ . Illustrated in Fig. 3 is a vehicular platoon, where the desired positions and the 'follower-leader' position errors, denoted as  $\tilde{x}_{i+1}$ , are showcased for each follower. This presentation spans the range of  $i=0, \dots, n-1$  (with  $n=5$  in this instance). Since state errors are calculated relative to the leading vehicle, we have  $\tilde{x}_0 = \dot{\tilde{x}}_0 = \ddot{\tilde{x}}_0 = 0$ .

### D. Platoon Targeted-Kinematics, and Controllers

The primary goal of the controller  $u_{i+1}$  in (2) is to achieve synchronization between the velocities and accelerations of the follower vehicles and those of the leading vehicle. Additionally, it aims to maintain desired distances between adjacent vehicles, denoted as  $d_i^{i+1}$ . To put it more straightforwardly, for each value of index  $i$  within the range from 0 to  $n-1$ , the controller has two main aims: firstly, to eliminate the 'follower-leader' state errors, and secondly, to align the velocity  $v_{i+1}$  and acceleration  $a_{i+1}$  with the velocity and acceleration of the leading vehicle, indicated as  $v_0$  and  $a_0$ , respectively. To accomplish this dual objective, a distributed linear control law [26] is utilized. The control law can be expressed using the following equations:

$$\begin{cases} u_{i+1} = - \sum_{j \in \mathbb{I}_{i+1}} k(\Delta x_{i+1}^j - d_{i+1,j}) + b \Delta \dot{x}_{i+1}^j + h \Delta \ddot{x}_{i+1}^j \\ d_{i+1,j} \triangleq -sgn(i+1-j) \sum_{\kappa=\min(i+1,j)}^{\max(i+1,j)-1} L_{\kappa} + d_{\kappa}^{\kappa+1} \end{cases} \quad (4)$$

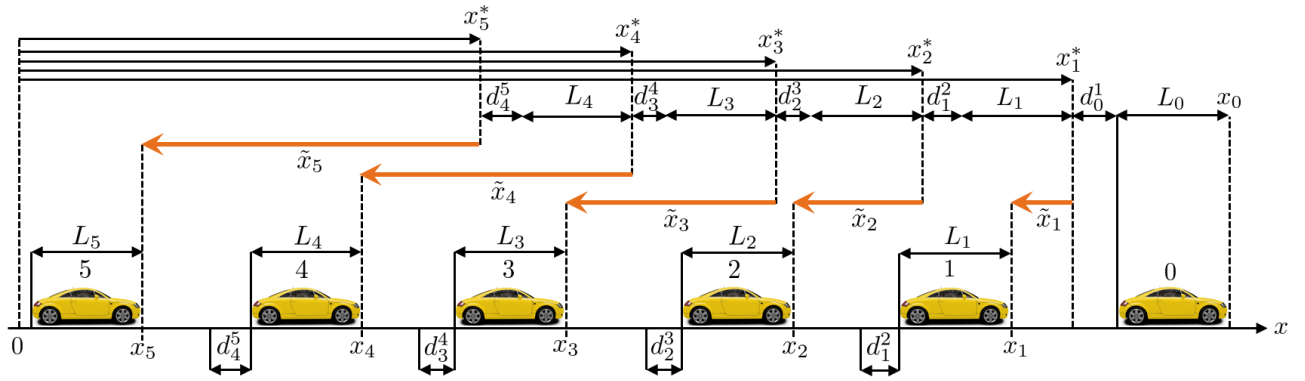


Fig. 3: Desired positions and ‘follower-leader’ position errors of the follower vehicles.

where  $\Delta x_{i+1}^j \triangleq x_{i+1} - x_j$ ,  $\Delta \dot{x}_{i+1}^j \triangleq \dot{x}_{i+1} - \dot{x}_j$ , and  $\Delta \ddot{x}_{i+1}^j \triangleq \ddot{x}_{i+1} - \ddot{x}_j$ . Considering that  $x_{i+1} - x_j - d_{i+1,j} = \tilde{x}_{i+1} - \tilde{x}_j$ ,  $\dot{x}_{i+1} - \dot{x}_j = \dot{\tilde{x}}_{i+1} - \dot{\tilde{x}}_j$ , and  $\ddot{x}_{i+1} - \ddot{x}_j = \ddot{\tilde{x}}_{i+1} - \ddot{\tilde{x}}_j$ , the controller (4) can be reformulated as:

$$u_{i+1} = - \sum_{j \in \mathbb{I}_{i+1}} \mathbf{K} (\tilde{\mathbf{X}}_{i+1} - \tilde{\mathbf{X}}_j) = - \sum_{j \in \mathbb{I}_{i+1}} \mathbf{K} \Delta \tilde{\mathbf{X}}_{i+1}^j \quad (5)$$

in which  $\Delta \tilde{\mathbf{X}}_{i+1}^j \triangleq \tilde{\mathbf{X}}_{i+1} - \tilde{\mathbf{X}}_j$  and the vector  $\mathbf{K} \triangleq [k, b, h]$  is introduced as the control-gain vector, which quantifies the impact of relative measurements between the  $(i+1)^{th}$  follower and the vehicles transmitting information to it.

### E. Platoon Dynamics, and Internal Stability

To find the platoon closed-loop dynamics, first noting that  $\ddot{x}_{i+1} = \ddot{\tilde{x}}_{i+1} + a_0$  and  $\ddot{x}_{i+1} = \ddot{\tilde{x}}_{i+1} + \dot{a}_0$ , and plugging (5) in (1), for  $i=0, \dots, n-1$ , yields

$$\ddot{\tilde{x}}_{i+1} = -\frac{1}{\tau} \mathbb{K}_{i+1} \tilde{\mathbf{X}}_{i+1} + \sum_{j \in \mathbb{I}_{i+1}} \frac{1}{\tau} \mathbf{K} \tilde{\mathbf{X}}_j + \epsilon_{i+1} \quad (6)$$

in which  $\epsilon_{i+1} \triangleq -\frac{1}{\tau} a_0(t) - \dot{a}_0(t)$  and  $\mathbb{K}_{i+1} \triangleq [k_{i+1}, \mathbf{b}_{i+1}, \mathbf{h}_{i+1}]$  such that

$$\mathbf{k}_{i+1} \triangleq |\mathbb{I}_{i+1}| k, \quad \mathbf{b}_{i+1} \triangleq |\mathbb{I}_{i+1}| b, \quad \mathbf{h}_{i+1} \triangleq 1 + |\mathbb{I}_{i+1}| h \quad (7)$$

where  $|\mathbb{I}_{i+1}|$  denotes the cardinality of the set  $\mathbb{I}_{i+1}$ . Now, considering (6), knowing  $\tilde{x}_0 = \dot{\tilde{x}}_0 = \ddot{\tilde{x}}_0 = 0$ , and defining the platoon’s total ‘follower-leader’ state-error vector by  $\tilde{\mathbf{X}}_t \triangleq [\tilde{\mathbf{X}}_1; \tilde{\mathbf{X}}_2; \dots; \tilde{\mathbf{X}}_n]$ , then the platoon’s closed-loop state-space dynamic model can be compactly characterized by

$$\dot{\tilde{\mathbf{X}}}_t = \underbrace{[\mathbf{I}_n \otimes \mathbf{A} - \mathbf{P} \otimes \mathbf{B} \mathbf{K}]}_{\triangleq \mathbf{A}_t} \tilde{\mathbf{X}}_t + \underbrace{\mathbf{I}_{3n}}_{\triangleq \mathbf{B}_t} \underbrace{\mathbf{Vec}(\epsilon_1, \epsilon_2, \dots, \epsilon_n)}_{\triangleq \mathbf{u}_t} \quad (8)$$

in which  $\mathbf{Vec}(\epsilon_1, \epsilon_2, \dots, \epsilon_n) = [\epsilon_1; \epsilon_2; \dots; \epsilon_n]$  where for  $i=0, \dots, n-1$ ,  $\epsilon_{i+1} \triangleq [0; 0; \epsilon_{i+1}]$ ,  $\mathbf{I}_{3n}$  is the identity matrix of size  $3n$ , and  $\mathbf{P} \in \mathbb{R}^{n \times n}$  whose elements  $p_{\kappa j}$  are according to

$$p_{\kappa j} = \begin{cases} |\mathbb{I}_{\kappa}| & \text{if } \kappa = j \\ 0 & \text{if } z_{\kappa}^j = 0 \\ -1 & \text{if } z_{\kappa}^j = 1 \end{cases} \quad (9)$$

where  $\kappa, j=1, \dots, n$  and  $|\mathbb{I}_{\kappa}|$  shows the cardinality of the set  $\mathbb{I}_{\kappa}$ .

**Remark 1:** Given (9) and Fig. 1, for BDCTs: BDL, BD and TBPF, since the communication between followers is undirected, i.e.,  $j \in \mathbb{I}_i \iff i \in \mathbb{I}_j$ ,  $i, j=1, \dots, n-1$ , then the matrix  $\mathbf{P}$  has only real eigenvalues ( $\lambda_i$ ,  $i=1, \dots, n$ ) [12]. Also, for BDCTs: TPSF and SPTF, the matrix  $\mathbf{P}$  has combination of real ( $\bar{\lambda}_i$ ,  $i=1, \dots, l$ ) and conjugate complex ( $\sigma_i \pm j\omega_i$ ,  $i=1, \dots, \frac{n-l}{2}$ ) eigenvalues [14].

**Remark 2:** For those BDCTs in which the matrix  $\mathbf{P}$  has only real eigenvalues, the platoon dynamics (8) would be asymptotically stable if and only if the resultant matrices

$$\mathbf{A} - \lambda_i \mathbf{B} \mathbf{K} \quad (10)$$

are all Hurwitz, i.e., their eigenvalues are all negative [12]. Note that  $\lambda_i$ ,  $i=1, \dots, n-1$ , denote the eigenvalues of the matrix  $\mathbf{P}$ . Given that  $k, b, h > 0$ , using Routh-Hurwitz stability criterion, the following condition can be found for the internal stability of the platoon:

$$b > \frac{k\tau}{1 + \lambda_{\min} h} \quad (11)$$

where  $\lambda_{\min} = \min_i \{\lambda_i\}$ .

**Remark 3:** For those BDCTs in which the eigenvalues of the matrix  $\mathbf{P}$  are combination of real and conjugate complex values, the platoon dynamics (8) would be asymptotically stable if and only if the following resultant matrices

$$\begin{cases} 1) \mathbf{A} - \bar{\lambda}_i \mathbf{B} \mathbf{K} & i=1, \dots, l \\ 2) \mathbf{I}_2 \otimes \mathbf{A} - \begin{bmatrix} \sigma_i & \omega_i \\ \omega_i & \sigma_i \end{bmatrix} \otimes \mathbf{B} \mathbf{K} & i=1, \dots, \frac{n-l}{2} \end{cases} \quad (12)$$

are all Hurwitz, i.e., their eigenvalues are all negative [14]. Note that in (12), the second matrix would result in a characteristic polynomial of degree six.

**Remark 4:** Internal stability in platooning ensures that vehicle states (positions, velocities, and accelerations) remain bounded over time for any bounded input. However, it does not guarantee collision-free distances between vehicles, as we will show with examples. Meeting internal stability conditions is crucial for stable platoon behavior but does not always prevent collisions or unsafe distances caused by control gains that meet these conditions. In simpler terms, relying solely on an internally stable platoon will not guarantee favorable

transient spacing between vehicles or even transient speeds and accelerations of the FVs. To reiterate, 'transient' simply pertains to the duration of trajectories before they reach their desired values.

**Remark 5:** Considering (8), when  $a_0(t)=0$ , we arrive at  $\dot{\tilde{\mathbf{X}}}_t = \mathbf{A}_t \tilde{\mathbf{X}}_t$ . Ensuring the internal stability conditions are met will lead to  $\tilde{\mathbf{X}}_t$  converging to zero in a steady state, which implies that  $x_{i+1}(t) = x_{i+1}^*(t)$ ,  $\dot{x}_{i+1}(t) = \dot{x}_{i+1}^*(t)$ , and  $\ddot{x}_{i+1}(t) = \ddot{x}_{i+1}^*(t)$  for  $i=0, \dots, n-1$ . However, if  $a_0 \neq 0$ , the control input  $\mathbf{u}_t$  will impact the convergence of IDs as well as the follower's velocities and accelerations toward their desired values. Nevertheless, we will demonstrate that by employing a state coordinate transformation, the new states associated with neighboring FVs, become independent of the leader vehicle's acceleration and jerk trajectories. Consequently, even if  $a_0 \neq 0$ , satisfying the internal stability conditions will still be sufficient for achieving convergence of IDs between FVs, velocities, and accelerations to their desired values.

#### IV. STATE COORDINATE TRANSFORMATION

Highlighting the platoon's dynamics, the closed-loop dynamics (8) emerges through the incorporation of established state errors between the 'follower' and 'leader' units. These errors are denoted as  $\tilde{\mathbf{X}}_{i+1}$  where  $i=0, \dots, n-1$ , and their visual representation (the position component) can be observed in Fig. 3. Nevertheless, achieving internal stability does not inherently safeguard against momentary variable distances among neighboring vehicles dropping below a safe threshold before attaining a desired intervehicle spacing. On the other hand, the 'follower-leader' state errors do not provide direct information about the state differences between adjacent vehicles. As such and as far as safety and collision concerned, we need to have a direct formulation for distance between every neighboring vehicles.

Adding to this, the visual representation of 'follower-leader' position errors, as evident in Fig. 3, not only lacks an intuitive portrayal of distances between adjacent vehicles but also inadequately facilitates direct analysis of transient intervehicle distances (TIDs). To establish a comprehensive framework surpassing internal stability considerations and fostering an intuitive TIDs examination, we undertake a transformation of previous state coordinates from 'follower-leader' errors to 'follower-predecessor' errors. This transformation yields 'follower-predecessor' errors derived from consecutive 'follower-leader' errors, exemplified in Fig. 4. An instance of this is the 'follower-predecessor' error between followers 1 and 2, derived from the 'follower#1-leader' and 'follower#2-leader' pairs.

According to this coordinate transformation, we introduce coupled position, velocity, acceleration, and jerk errors between neighboring vehicles  $i$  and  $i+1$  as follows: 1. Coupled position error: Denoted as  $\Delta \tilde{p}_i^{i+1} \triangleq \tilde{x}_i - \tilde{x}_{i+1}$ , representing the difference in position errors. 2. Coupled velocity error: Denoted as  $\Delta \tilde{v}_i^{i+1} \triangleq \dot{\tilde{x}}_i - \dot{\tilde{x}}_{i+1}$ , signifying the difference in velocity errors. 3. Coupled acceleration error: Denoted as  $\Delta \tilde{a}_i^{i+1} \triangleq \ddot{\tilde{x}}_i - \ddot{\tilde{x}}_{i+1}$ , representing the difference in acceleration errors. 4. Coupled jerk error: Denoted as  $\Delta \tilde{j}_i^{i+1} \triangleq \ddot{\tilde{x}}_i - \ddot{\tilde{x}}_{i+1}$ ,

indicating the difference in jerk errors. With these formulations, the 'follower-predecessor' state error and its derivative for neighboring vehicles  $i$  and  $i+1$  can be expressed as follows:

$$\begin{aligned} \Delta \tilde{\mathbf{X}}_i^{i+1} &\triangleq \tilde{\mathbf{X}}_i - \tilde{\mathbf{X}}_{i+1} \triangleq [\Delta \tilde{p}_i^{i+1}; \Delta \tilde{v}_i^{i+1}; \Delta \tilde{a}_i^{i+1}] \\ \Delta \dot{\tilde{\mathbf{X}}}_i^{i+1} &\triangleq \dot{\tilde{\mathbf{X}}}_i - \dot{\tilde{\mathbf{X}}}_{i+1} \triangleq [\Delta \dot{\tilde{p}}_i^{i+1}; \Delta \dot{\tilde{v}}_i^{i+1}; \Delta \dot{\tilde{a}}_i^{i+1}] \end{aligned} \quad (13)$$

Using these error terms, we derive the coupled distance dynamics governing neighboring vehicles in BDCTs. We will refer to  $\Delta \tilde{p}_i^{i+1}(\cdot)$  as the transient intervehicle distance error (TIDE) between vehicles  $i$  and  $i+1$  in both the time and Laplace domains (please see Fig. 5 for visual presentation of coupled position errors). Importantly, for instance, 'follower-predecessor' state errors between vehicles  $i$  and  $j$  (where  $j > i$ ) can be expressed as  $\Delta \tilde{\mathbf{X}}_i^j \triangleq \tilde{\mathbf{X}}_i - \tilde{\mathbf{X}}_j$ .

#### V. PLATOON DISTANCE DYNAMIC MODEL

In this section, we present an alternative dynamic model based on (8), sharing the previously mentioned internal stability conditions (Remarks 2-3). This model enables the examination of TIDEs and the determination of control gains to prevent collisions and maintain safe spacing between vehicles. To find the coupled dynamics of pairwise neighboring vehicles  $i$  and  $i+1$ , we need  $\Delta \tilde{j}_i^{i+1}$  for  $i=0, 1, \dots, n-1$ .

**Theorem 1:** For  $i=0, \dots, n-1$ , the coupled jerk error between neighboring vehicles  $i$  and  $i+1$  under BDCTs (Fig. 3) is given by:

$$\begin{aligned} \Delta \tilde{j}_i^{i+1} &= -\frac{1}{\tau} \mathbb{J}_i \Delta \tilde{\mathbf{X}}_i^{i+1} + \frac{1}{\tau} \mathbf{K} \sum_{j \in \alpha_i} \sum_{\kappa=j}^{i-1} \Delta \tilde{\mathbf{X}}_{\kappa}^{\kappa+1} \\ &+ \frac{1}{\tau} \mathbf{K} \sum_{j \in \beta_i} \sum_{\kappa=i+1}^{j-1} \Delta \tilde{\mathbf{X}}_{\kappa}^{\kappa+1} - U(0.5-i) \epsilon_{i+1} \end{aligned} \quad (14)$$

In this equation,  $U(\cdot)$  is the unit step function, and  $\mathbb{J}_i$  is defined as  $[|\mathbf{J}_i|k, |\mathbf{J}_i|b, 1+|\mathbf{J}_i|h]$ , where  $|\mathbf{J}_i|$  is determined as follows:

$$|\mathbf{J}_i| = \begin{cases} |\mathbb{I}_i| & \text{if } \beta_i = \emptyset \text{ \& } i \neq 0 \\ 1 & \text{if } i = 0 \\ |\mathbb{I}_{i+1}| & \text{if } \beta_i \neq \emptyset \text{ \& } i \neq 0 \end{cases} \quad (15)$$

The sets  $\alpha_i$  and  $\beta_i$  are defined as  $\alpha_i \triangleq \{j \in \mathbb{R}_i \mid z_i^j = 1 \text{ \& } z_{i+1}^j = 0 \text{ \& } j < i\}$  and  $\beta_i \triangleq \{j \in \mathbb{R}_{i+1} \mid z_{i+1}^j = 1 \text{ \& } z_i^j = 0 \text{ \& } j > i+1\}$ , respectively. Refer to Table I for sets  $\alpha_i$ ,  $\beta_i$ , and  $|\mathbb{I}_{i+1}|$  values for the platoon under BDCTs (Fig. 1).

**Proof:** For  $i=1, \dots, n-1$ , using (6), we have

$$\begin{cases} \ddot{\tilde{x}}_i = -\frac{1}{\tau} \mathbb{K}_i \tilde{\mathbf{X}}_i + \frac{1}{\tau} \sum_{j \in \mathbb{I}_i} \mathbf{K} \tilde{\mathbf{X}}_j + \epsilon_i \\ \ddot{\tilde{x}}_{i+1} = -\frac{1}{\tau} \mathbb{K}_{i+1} \tilde{\mathbf{X}}_{i+1} + \frac{1}{\tau} \sum_{j \in \mathbb{I}_{i+1}} \mathbf{K} \tilde{\mathbf{X}}_j + \epsilon_{i+1} \end{cases} \quad (16)$$

Therefore, given  $\epsilon_i = \epsilon_{i+1}$  and  $\Delta \tilde{j}_i^{i+1} \triangleq \ddot{\tilde{x}}_i - \ddot{\tilde{x}}_{i+1}$ , we get

$$\begin{aligned} \Delta \tilde{j}_i^{i+1} &= -\frac{1}{\tau} \mathbb{K}_i \Delta \tilde{\mathbf{X}}_i^{i+1} - \frac{1}{\tau} (\mathbb{K}_i - \mathbb{K}_{i+1}) \tilde{\mathbf{X}}_{i+1} \\ &+ \sum_{j \in \mathbb{I}_i} \frac{1}{\tau} \mathbf{K} \tilde{\mathbf{X}}_j - \sum_{j \in \mathbb{I}_{i+1}} \frac{1}{\tau} \mathbf{K} \tilde{\mathbf{X}}_j \end{aligned} \quad (17)$$

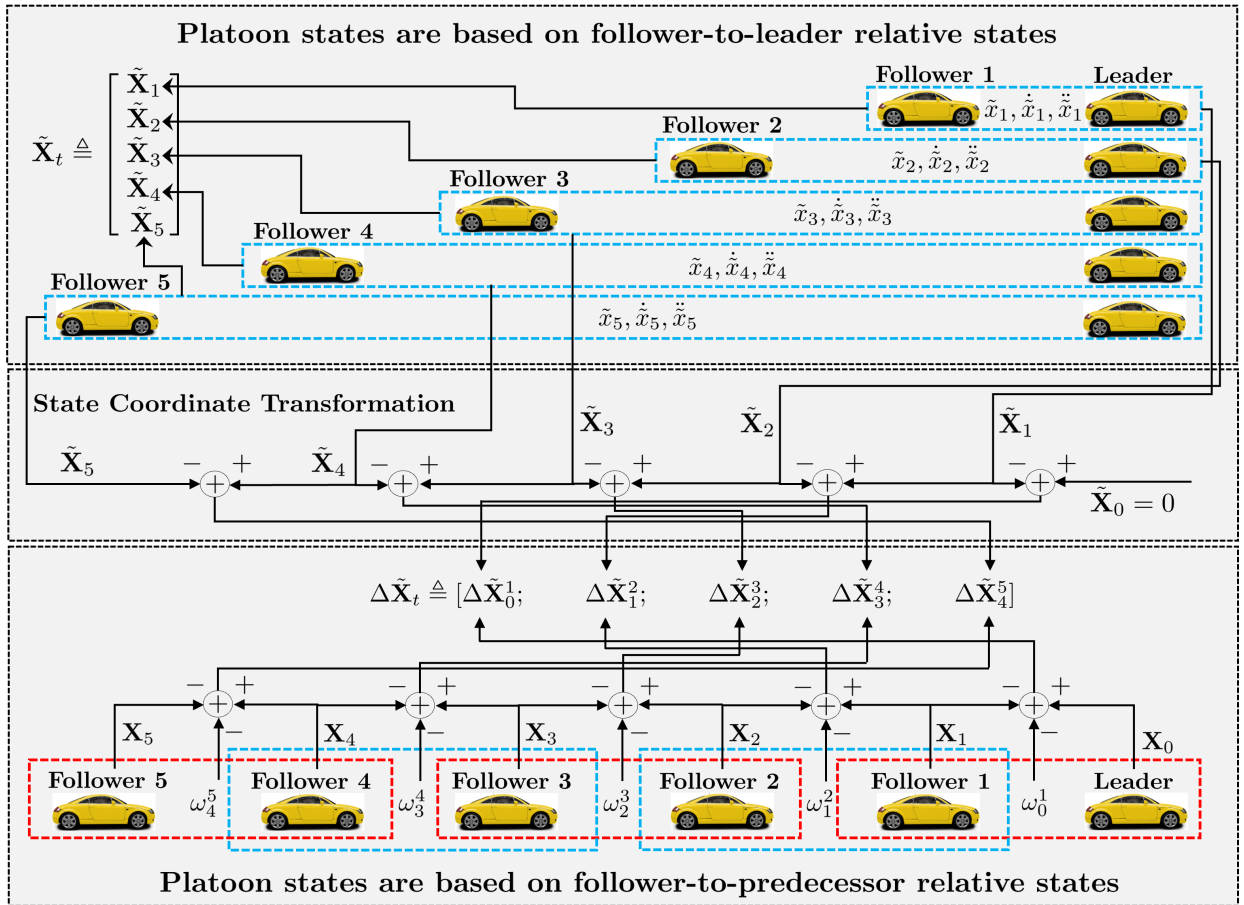


Fig. 4: State coordinate transformation from ‘follower-leader’ errors to ‘follower-predecessor’ errors.

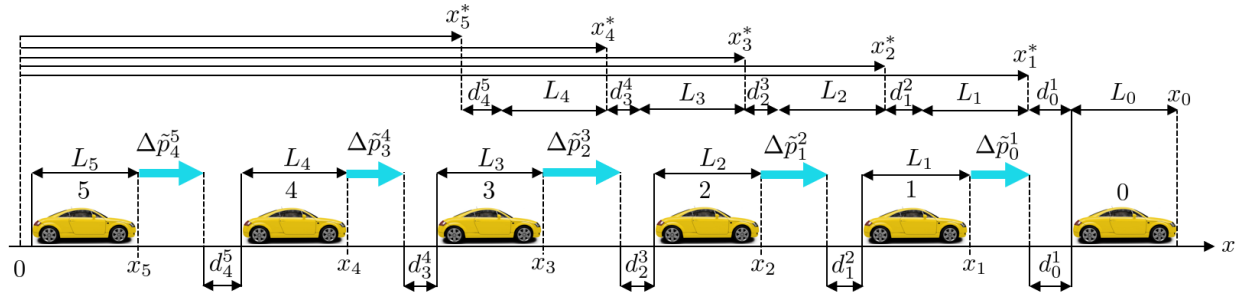


Fig. 5: Desired positions and ‘follower-predecessor’ position errors of the follower vehicles.

Since  $-\frac{1}{\tau}(\mathbb{K}_i - \mathbb{K}_{i+1}) = \sum_{j \in \mathbb{I}_{i+1}} \frac{1}{\tau} \mathbf{K} - \sum_{j \in \mathbb{I}_i} \frac{1}{\tau} \mathbf{K}$  then (17) can be rewritten as

$$\Delta \tilde{\mathbf{J}}_i^{i+1} = -\frac{1}{\tau} \mathbb{K}_i \Delta \tilde{\mathbf{X}}_i^{i+1} + \sum_{j \in \mathbb{I}_i} \frac{1}{\tau} \mathbf{K} \Delta \tilde{\mathbf{X}}_j^{i+1} - \sum_{j \in \mathbb{I}_{i+1}} \frac{1}{\tau} \mathbf{K} \Delta \tilde{\mathbf{X}}_j^{i+1} \quad (18)$$

Also, as  $\tilde{\mathbf{X}}_j - \tilde{\mathbf{X}}_{i+1} = \tilde{\mathbf{X}}_j - \tilde{\mathbf{X}}_i + \tilde{\mathbf{X}}_i - \tilde{\mathbf{X}}_{i+1}$ , (18) can be reformulated as

$$\begin{aligned} \Delta \tilde{\mathbf{J}}_i^{i+1} = & \frac{1}{\tau} \left( -(\mathbb{K}_i + \mathbf{K}) + \sum_{j \in \mathbb{R}_i} \mathbf{K} - \sum_{j \in \mathbb{R}_{i+1}} \mathbf{K} \right) \Delta \tilde{\mathbf{X}}_i^{i+1} \\ & + \sum_{j \in \mathbb{R}_i} \frac{1}{\tau} \mathbf{K} \Delta \tilde{\mathbf{X}}_j^i - \sum_{j \in \mathbb{R}_{i+1}} \frac{1}{\tau} \mathbf{K} \Delta \tilde{\mathbf{X}}_j^i \end{aligned} \quad (19)$$

Note that for the given BDCTs we have  $\mathbb{I}_i = \mathbb{R}_i \cup \{i+1\}$  and  $\mathbb{I}_{i+1} = \mathbb{R}_{i+1} \cup \{i\}$ . Splitting  $j \in \mathbb{R}_i$  and  $j \in \mathbb{R}_{i+1}$  in two parts, i.e.,  $j < i$  and  $j > i+1$ , and using the fact that for part  $j > i+1$ , we have  $\mathbf{X}_j - \tilde{\mathbf{X}}_i = \mathbf{X}_j - \tilde{\mathbf{X}}_{i+1} - (\tilde{\mathbf{X}}_i - \tilde{\mathbf{X}}_{i+1})$ , (19) can be reformulated as

$$\begin{aligned} \Delta \tilde{\mathbf{J}}_i^{i+1} = & \frac{1}{\tau} \left( -(\mathbb{K}_i + \mathbf{K}) + \sum_{j \in \mathbb{R}_i < i} \mathbf{K} - \sum_{j \in \mathbb{R}_{i+1} < i} \mathbf{K} \right) \Delta \tilde{\mathbf{X}}_i^{i+1} \\ & + \sum_{j \in \mathbb{R}_i < i} \frac{1}{\tau} \mathbf{K} \Delta \tilde{\mathbf{X}}_j^i - \sum_{j \in \mathbb{R}_{i+1} < i} \frac{1}{\tau} \mathbf{K} \Delta \tilde{\mathbf{X}}_j^i \\ & + \sum_{j \in \mathbb{R}_{i+1} > i+1} \frac{1}{\tau} \mathbf{K} \Delta \tilde{\mathbf{X}}_{i+1}^j - \sum_{j \in \mathbb{R}_i > i+1} \frac{1}{\tau} \mathbf{K} \Delta \tilde{\mathbf{X}}_{i+1}^j \end{aligned} \quad (20)$$

TABLE I: Sets  $\alpha_i$  and  $\beta_i$ , and values of  $|\mathbb{I}_{i+1}|$  and  $|\mathbf{J}_i|$  for the platoon and BDCTs given in Fig. 1.

Pairs:	(0,1)	(1,2)	(2,3)	(3,4)	(4,5)
	$\{\alpha_0, \beta_0\}$ & $ \mathbb{I}_1 $ & $ \mathbf{J}_0 $	$\{\alpha_1, \beta_1\}$ & $ \mathbb{I}_2 $ & $ \mathbf{J}_1 $	$\{\alpha_2, \beta_2\}$ & $ \mathbb{I}_3 $ & $ \mathbf{J}_2 $	$\{\alpha_3, \beta_3\}$ & $ \mathbb{I}_4 $ & $ \mathbf{J}_3 $	$\{\alpha_4, \beta_4\}$ & $ \mathbb{I}_5 $ & $ \mathbf{J}_4 $
<b>BDL</b>	$\{\emptyset, \{2\}\}$ & 2 & 1	$\{\emptyset, \{3\}\}$ & 3 & 3	$\{\{1\}, \{4\}\}$ & 3 & 3	$\{\{2\}, \{5\}\}$ & 3 & 3	$\{\{3\}, \emptyset\}$ & 2 & 3
<b>BD</b>	$\{\emptyset, \{2\}\}$ & 2 & 1	$\{\{0\}, \{3\}\}$ & 2 & 2	$\{\{1\}, \{4\}\}$ & 2 & 2	$\{\{2\}, \{5\}\}$ & 2 & 2	$\{\{3\}, \emptyset\}$ & 1 & 2
<b>TBPF</b>	$\{\emptyset, \{2,3\}\}$ & 3 & 1	$\{\emptyset, \{4\}\}$ & 4 & 4	$\{\{0\}, \{5\}\}$ & 4 & 4	$\{\{1\}, \emptyset\}$ & 3 & 4	$\{\{2\}, \emptyset\}$ & 2 & 3
<b>TPSF</b>	$\{\emptyset, \{2\}\}$ & 2 & 1	$\{\emptyset, \{3\}\}$ & 3 & 3	$\{\{0\}, \{4\}\}$ & 3 & 3	$\{\{1\}, \{5\}\}$ & 3 & 3	$\{\{2\}, \emptyset\}$ & 2 & 3
<b>SPTF</b>	$\{\emptyset, \{2,3\}\}$ & 3 & 1	$\{\{0\}, \{4\}\}$ & 3 & 3	$\{\{1\}, \{5\}\}$ & 3 & 3	$\{\{2\}, \emptyset\}$ & 2 & 3	$\{\{3\}, \emptyset\}$ & 1 & 2

**Remark 6:** In the context of the provided BDCTs, when we examine any pair  $(i, i+1)$ , one of the following conditions holds: 1. Both the  $i^{\text{th}}$  and  $(i+1)^{\text{th}}$  vehicles receive information from vehicles either ahead or behind them. 2. Only the  $i^{\text{th}}$  vehicle receives information from specific vehicles ahead, while the  $(i+1)^{\text{th}}$  vehicle does not. 3. Only the  $(i+1)^{\text{th}}$  vehicle acquires information from specific vehicles behind, while the  $i^{\text{th}}$  vehicle does not. For instance, considering the pair (2,3) in the TPSF topology shown in Fig. 1, both vehicles 2 and 3 receive information from vehicle 1. Vehicle 2 obtains information from the leader vehicle, while vehicle 3 does not. Additionally, vehicle 3 receives information from vehicle 4, and vehicle 2 does not.

Given Remark 6, and sets  $\alpha_i$  and  $\beta_i$ , (20) can be simplified to

$$\Delta \tilde{\mathbf{J}}_i^{i+1} = \frac{1}{\tau} \left( -(\mathbb{K}_i + \mathbf{K}) + \sum_{j \in \alpha_i} \mathbf{K} \right) \Delta \tilde{\mathbf{X}}_i^{i+1} + \sum_{j \in \alpha_i} \frac{1}{\tau} \mathbf{K} \Delta \tilde{\mathbf{X}}_j^i + \sum_{j \in \beta_i} \frac{1}{\tau} \mathbf{K} \Delta \tilde{\mathbf{X}}_{i+1}^j \quad (21)$$

Having  $|\alpha_i|$  as the cardinality of the set  $\alpha_i$ , (21) can be reformulated as

$$\Delta \tilde{\mathbf{J}}_i^{i+1} = -\frac{1}{\tau} (\mathbb{K}_i + \mathbf{K} - |\alpha_i| \mathbf{K}) \Delta \tilde{\mathbf{X}}_i^{i+1} + \sum_{j \in \alpha_i} \frac{1}{\tau} \mathbf{K} \Delta \tilde{\mathbf{X}}_j^i + \sum_{j \in \beta_i} \frac{1}{\tau} \mathbf{K} \Delta \tilde{\mathbf{X}}_{i+1}^j \quad (22)$$

On the other hand, for  $i=1, \dots, n-1$  and BDCTs, we have

$$\begin{cases} |\mathbb{I}_{i+1}| = |\mathbb{I}_i| - 1 & \& \; |\alpha_i| = 1 & \text{if } \beta_i = \emptyset \\ |\mathbb{I}_{i+1}| = |\mathbb{I}_i| + (1 - |\alpha_i|) & \& \; |\beta_i| = 1 & \text{if } \beta_i \neq \emptyset \end{cases} \quad (23)$$

which implies that

$$\mathbb{K}_i + \mathbf{K} - |\alpha_i| \mathbf{K} = \begin{cases} \mathbb{K}_i & \text{if } \beta_i = \emptyset \\ \mathbb{K}_{i+1} & \text{if } \beta_i \neq \emptyset \end{cases} \quad (24)$$

Therefore, given (23), (22) can be rewritten as

$$\Delta \tilde{\mathbf{J}}_i^{i+1} = \begin{cases} -\frac{1}{\tau} \mathbb{K}_i \Delta \tilde{\mathbf{X}}_i^{i+1} + \sum_{j \in \alpha_i} \frac{1}{\tau} \mathbf{K} \Delta \tilde{\mathbf{X}}_j^i; & \beta_i = \emptyset \\ -\frac{1}{\tau} \mathbb{K}_{i+1} \Delta \tilde{\mathbf{X}}_i^{i+1} + \sum_{j \in \alpha_i} \frac{1}{\tau} \mathbf{K} \Delta \tilde{\mathbf{X}}_j^i & \\ + \sum_{j \in \beta_i} \frac{1}{\tau} \mathbf{K} \Delta \tilde{\mathbf{X}}_{i+1}^j & ; \beta_i \neq \emptyset \end{cases} \quad (25)$$

Now, given that for the pair  $(i, i+1)$ ,  $\Delta \tilde{\mathbf{X}}_j^i$  and  $\Delta \tilde{\mathbf{X}}_{i+1}^j$  can be rewritten in the following form:

$$\begin{cases} \Delta \tilde{\mathbf{X}}_j^i = \sum_{\kappa=j}^{i-1} \Delta \tilde{\mathbf{X}}_{\kappa}^{\kappa+1}; & j < i \\ \Delta \tilde{\mathbf{X}}_{i+1}^j = \sum_{\kappa=i+1}^{j-1} \Delta \tilde{\mathbf{X}}_{\kappa}^{\kappa+1}; & j > i+1 \end{cases} \quad (26)$$

then substituting (26) into (25) yields

$$\Delta \tilde{\mathbf{J}}_i^{i+1} = \begin{cases} -\frac{1}{\tau} \mathbb{K}_i \Delta \tilde{\mathbf{X}}_i^{i+1} + \frac{1}{\tau} \mathbf{K} \sum_{j \in \alpha_i} \sum_{\kappa=j}^{i-1} \Delta \tilde{\mathbf{X}}_{\kappa}^{\kappa+1}; & \beta_i = \emptyset \\ -\frac{1}{\tau} \mathbb{K}_{i+1} \Delta \tilde{\mathbf{X}}_i^{i+1} + \frac{1}{\tau} \mathbf{K} \sum_{j \in \alpha_i} \sum_{\kappa=j}^{i-1} \Delta \tilde{\mathbf{X}}_{\kappa}^{\kappa+1} & \\ + \frac{1}{\tau} \mathbf{K} \sum_{j \in \beta_i} \sum_{\kappa=i+1}^{j-1} \Delta \tilde{\mathbf{X}}_{\kappa}^{\kappa+1} & ; \beta_i \neq \emptyset \end{cases} \quad (27)$$

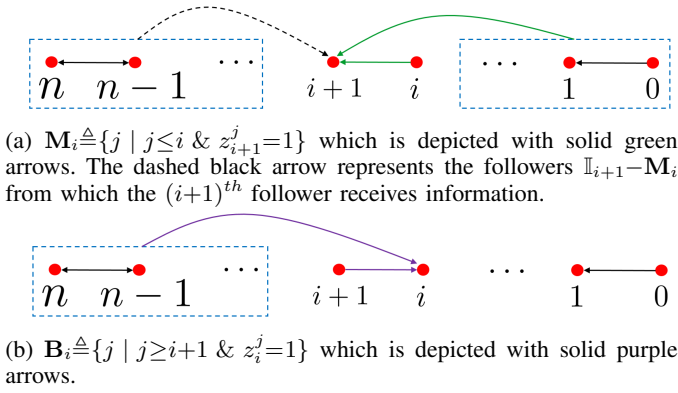
Now, let us study the pair (0,1). For the given BDCTs, given that  $\tilde{\mathbf{X}}_0 = 0$  we have

$$\begin{aligned} \Delta \tilde{\mathbf{J}}_0^1 &= -\frac{1}{\tau} \mathbb{K}_1 \Delta \tilde{\mathbf{X}}_0^1 - \frac{1}{\tau} \sum_{j \in \mathbb{R}_1} \mathbf{K} \tilde{\mathbf{X}}_{j-1} \\ &= -\frac{1}{\tau} \mathbb{K}_1 \Delta \tilde{\mathbf{X}}_0^1 + \frac{1}{\tau} \sum_{j \in \mathbb{R}_1} \mathbf{K} (\Delta \tilde{\mathbf{X}}_0^1 + \Delta \tilde{\mathbf{X}}_1^j) - \epsilon_1 \\ &= -\frac{1}{\tau} (\mathbb{K}_1 - |\beta_0| \mathbf{K}) \Delta \tilde{\mathbf{X}}_0^1 + \frac{1}{\tau} \sum_{j \in \beta_0} \mathbf{K} \Delta \tilde{\mathbf{X}}_1^j - \epsilon_1 \end{aligned} \quad (28)$$

where  $\beta_0 \triangleq \{j \in \mathbb{R}_1 \mid j \geq 2\}$ . Also, for the pair (0,1), since  $|\beta_0| = |\mathbb{I}_1| - (1 - |\alpha_0|)$ , then  $\mathbb{K}_1 - |\beta_0| \mathbf{K} = \mathbb{K}$ , where  $\mathbb{K} \triangleq [k, b, 1+h]$ . Therefore, (28) can be rewritten as

$$\Delta \tilde{\mathbf{J}}_0^1 = -\frac{1}{\tau} \mathbb{K} \Delta \tilde{\mathbf{X}}_0^1 + \frac{1}{\tau} \mathbf{K} \sum_{j \in \beta_0} \sum_{\kappa=1}^{j-1} \Delta \tilde{\mathbf{X}}_{\kappa}^{\kappa+1} - \epsilon_1 \quad (29)$$

Subsequently (27) and (29) can be unified as a single formula. Let the set  $\mathbf{J}_i$  be defined as  $\mathbf{J}_i \triangleq \{j \mid j \leq i \& z_{i+1}^j = 1\} \cup \{j \mid j \geq i+1 \& z_i^j = 1\}$ ;  $i=0, \dots, n-1$ . For  $i=1, \dots, n-1$ , first we split the set  $\mathbf{J}_i$  in two sets:  $\mathbf{M}_i \triangleq \{j \mid j \leq i \& z_{i+1}^j = 1\}$  and  $\mathbf{B}_i \triangleq \{j \mid j \geq i+1 \& z_i^j = 1\}$ , such that  $\mathbf{J}_i = \mathbf{M}_i \cup \mathbf{B}_i$ . Figs. 6a-6b depicts these sets, respectively.


 Fig. 6: Illustration of sets  $\mathbf{M}_i$  and  $\mathbf{B}_i$ 

Regarding the definition  $\beta_i \triangleq \{j \in \mathbb{R}_{i+1} \mid z_{i+1}^j = 1 \text{ \& } z_i^j = 0 \text{ \& } j > i+1\}$ , we have two cases for the pair  $(i, i+1)$ ;  $i = 1, \dots, n-1$ :

**Case 1:**  $\beta_i = \emptyset$

Having  $\beta_i = \emptyset$  implies that the followers behind from which the  $(i+1)^{th}$  follower receives information (the followers  $\mathbb{I}_{i+1} - \mathbf{M}_i$ , see Fig. 6a), also send information to the  $i^{th}$  follower. Therefore, the set  $\mathbf{B}_i$  (see Fig. 6b) can be obtained as  $\mathbf{B}_i = \{i+1\} \cup (\mathbb{I}_{i+1} - \mathbf{M}_i)$ . It is clear that  $|\mathbf{J}_i| = |\mathbf{M}_i| + |\mathbf{B}_i|$  in which  $|\cdot|$  denotes the cardinality of the sets. As such, we have  $|\mathbf{B}_i| = 1 + |\mathbb{I}_{i+1}| - |\mathbf{M}_i|$  and, therefore,  $|\mathbf{J}_i| = 1 + |\mathbb{I}_{i+1}| = |\mathbb{I}_i|$  (see (23)).

**Case 2:**  $\beta_i \neq \emptyset$

Having  $\beta_i \neq \emptyset$  implies that the followers behind (other than the  $(i+1)^{th}$  follower) from which the  $i^{th}$  follower receives information are only  $\mathbb{I}_{i+1} - \mathbf{M}_i - \beta_i$ . Therefore,  $\mathbf{B}_i = \{i+1\} \cup (\mathbb{I}_{i+1} - \mathbf{M}_i - \beta_i)$ , and thus  $|\mathbf{B}_i| = 1 + |\mathbb{I}_{i+1}| - |\mathbf{M}_i| - |\beta_i|$  and  $|\mathbf{J}_i| = |\mathbf{M}_i| + |\mathbf{B}_i| = 1 + |\mathbb{I}_{i+1}| - |\beta_i| = |\mathbb{I}_{i+1}|$  (see (23)).

Finally, given the definition of the set  $\mathbf{J}_i$ , we always have  $\mathbf{J}_0 = \{0\}$  and therefore  $|\mathbf{J}_0| = 1$ . Thus, for  $i = 0, \dots, n-1$ , (27) and (29) can be unified and the unified coupled jerk error between the neighboring vehicles  $i$  and  $i+1$  under the BDCTs given in Fig. 3 would be according to (14). Therefore, the proof completed. ■

**Theorem 2:** The state errors of ‘follower-leader’ pairs and the state errors of neighboring ‘follower-predecessor’ pairs are governed by a shared internal stability condition.

**Proof:** Considering (14), regarding the facts that  $d/dt\{\Delta\tilde{p}_i^{i+1}\} = \Delta\tilde{v}_i^{i+1}$  and  $d/dt\{\Delta\tilde{v}_i^{i+1}\} = \Delta\tilde{a}_i^{i+1}$ , assuming  $\Delta\tilde{y}_i^{i+1} = \Delta\tilde{p}_i^{i+1}$  as the output of the pairs coupled dynamics, then for  $i = 0, \dots, n-1$ , the state-space model for the pair  $(i, i+1)$  can be presented as

$$\begin{cases} \Delta\dot{\tilde{\mathbf{X}}}_i^{i+1} = \mathbf{A}_i^{i+1} \Delta\tilde{\mathbf{X}}_i^{i+1} + \mathbf{B}_i^{i+1} \Delta\tilde{u}_i^{i+1} \\ \Delta\tilde{y}_i^{i+1} = \mathbf{C}_i^{i+1} \Delta\tilde{\mathbf{X}}_i^{i+1} \end{cases} \quad (30)$$

where  $\mathbf{C}_i^{i+1} = [1, 0, 0]$ ,  $\mathbf{B}_i^{i+1} = \mathbf{B}$ , and  $\mathbf{A}_i^{i+1} \in R^{3 \times 3}$  and  $\tilde{u}_i^{i+1} \in R$  are

$$\mathbf{A}_i^{i+1} = \begin{bmatrix} 0 & 1 & 0 \\ 0 & 0 & 1 \\ -\frac{|\mathbf{J}_i|k}{\tau} & -\frac{|\mathbf{J}_i|b}{\tau} & -\frac{1+|\mathbf{J}_i|h}{\tau} \end{bmatrix} \quad (31)$$

and

$$\Delta\tilde{u}_i^{i+1} = \mathbf{K} \sum_{j \in \alpha_i, \kappa=j}^{i-1} \tilde{\mathbf{X}}_{\kappa}^{\kappa+1} + \mathbf{K} \sum_{j \in \beta_i, \kappa=i+1}^{j-1} \tilde{\mathbf{X}}_{\kappa}^{\kappa+1} - U(0.5-i)\epsilon_{i+1} \quad (32)$$

respectively. Note that the sets  $\mathbf{J}_i$ ,  $\alpha_i$  and  $\beta_i$  are mutually disjoint, i.e.,  $\mathbf{J}_i \cap \alpha_i = \emptyset$ ,  $\mathbf{J}_i \cap \beta_i = \emptyset$  and  $\alpha_i \cap \beta_i = \emptyset$ . Also, always  $\alpha_0 = \emptyset$  and  $\beta_{n-1} = \emptyset$ . Defining  $\Delta\tilde{\mathbf{X}}_t \in R^{3n \times 1} = [\Delta\tilde{\mathbf{X}}_0^1; \Delta\tilde{\mathbf{X}}_1^2; \dots; \Delta\tilde{\mathbf{X}}_{n-1}^n]$ , applying  $i = 0, \dots, n-1$  to the first relation in (30), the stacked resultant relations can be compactly shown as

$$\Delta\dot{\tilde{\mathbf{X}}}_t = \underbrace{[\mathbf{I}_n \otimes \mathbf{A} - \bar{\mathbf{P}} \otimes \mathbf{BK}]}_{\triangleq \tilde{\mathbf{A}}_{t\Delta}} \Delta\tilde{\mathbf{X}}_t + \mathbf{I}_{3n} \mathbf{Vec}(-\epsilon_1, \mathbf{0}, \dots, \mathbf{0}) \quad (33)$$

where  $\mathbf{0} \triangleq [0; 0; 0]$ , and  $\bar{\mathbf{P}} \in R^{n \times n}$  whose elements,  $\bar{p}_{ij}$ , are according to

$$\bar{p}_{ij} = \begin{cases} -|\mathbb{S}_j \cap \alpha_{i-1}| & \text{if } j < i \\ |\mathbf{J}_{i-1}| & \text{if } j = i \\ -|\mathbb{V}_j \cap \beta_{i-1}| & \text{if } j > i \end{cases} \quad (34)$$

where  $|\cdot|$  denotes the cardinality of the relevant sets,  $\mathbb{S}_j \triangleq \{j-1, j-2, \dots, 0\}$  and  $\mathbb{V}_j \triangleq \{j, j+1, \dots, n\}$ . Also,  $\bar{p}_{ij} = 0$  for the cases  $\mathbb{S}_j \cap \alpha_{i-1} = \emptyset$  and  $\mathbb{V}_j \cap \beta_{i-1} = \emptyset$ . Fig. 7, illustrates the platoon dynamics (8) which has been developed by using the ‘follower-leader’ state errors, and the alternative dynamics (33) which obtained after state coordinate transformation and utilizing neighboring ‘follower-predecessor’ state errors.

Following (9) and (34), for any BDCT depicted in Fig. 1, the eigenvalues of the matrices  $\mathbf{P}$  and  $\bar{\mathbf{P}}$  are identical. For instance, for the case of having five followers and using TBPF topology, the matrices are

$$\mathbf{P} = \begin{bmatrix} 3 & -1 & -1 & 0 & 0 \\ -1 & 4 & -1 & -1 & 0 \\ -1 & -1 & 4 & -1 & -1 \\ 0 & -1 & -1 & 3 & -1 \\ 0 & 0 & -1 & -1 & 2 \end{bmatrix}, \quad \bar{\mathbf{P}} = \begin{bmatrix} 1 & -2 & -1 & 0 & 0 \\ 0 & 4 & -1 & -1 & 0 \\ -1 & -1 & 4 & -1 & -1 \\ 0 & -1 & -1 & 4 & 0 \\ 0 & 0 & -1 & -1 & 3 \end{bmatrix} \quad (35)$$

both of which have eigenvalues: 0.2935, 2.1324, 3.3900, 5.0000 and 5.1841 and thus are similar matrices. Please check Link for matrices  $\mathbf{P}$  and  $\bar{\mathbf{P}}$  of the other BDCTs. Considering (8), (33), and the fact that  $a_0(t)$  is bounded, since the system matrices  $\tilde{\mathbf{A}}_t$  and  $\tilde{\mathbf{A}}_{t\Delta}$  are in similar formats as

$$\tilde{\mathbf{A}}_t = [\mathbf{I}_n \otimes \mathbf{A} - \mathbf{P} \otimes \mathbf{BK}] \quad (36a)$$

$$\tilde{\mathbf{A}}_{t\Delta} = [\mathbf{I}_n \otimes \mathbf{A} - \bar{\mathbf{P}} \otimes \mathbf{BK}] \quad (36b)$$

and regarding the property that  $\mathbf{P}$  and  $\bar{\mathbf{P}}$  are similar, dynamics (33) can be utilized instead of (8) for internal stability analysis. Therefore, the two cases mentioned earlier in the Remarks 2-3 are valid for the matrix  $\bar{\mathbf{P}}$  as well. Thus the proof completed. ■

## VI. TRANSIENT INTERVEHICLE DISTANCE ERRORS (TIDES)

Given (14) and BDCTs in Fig. 1, there is a coupling between the pair  $(i, i+1)$  and the pairs in the set  $(\cup_{j \in \alpha_i} \cup_{\kappa=j}^{i-1} \zeta_{\kappa}) \cup$

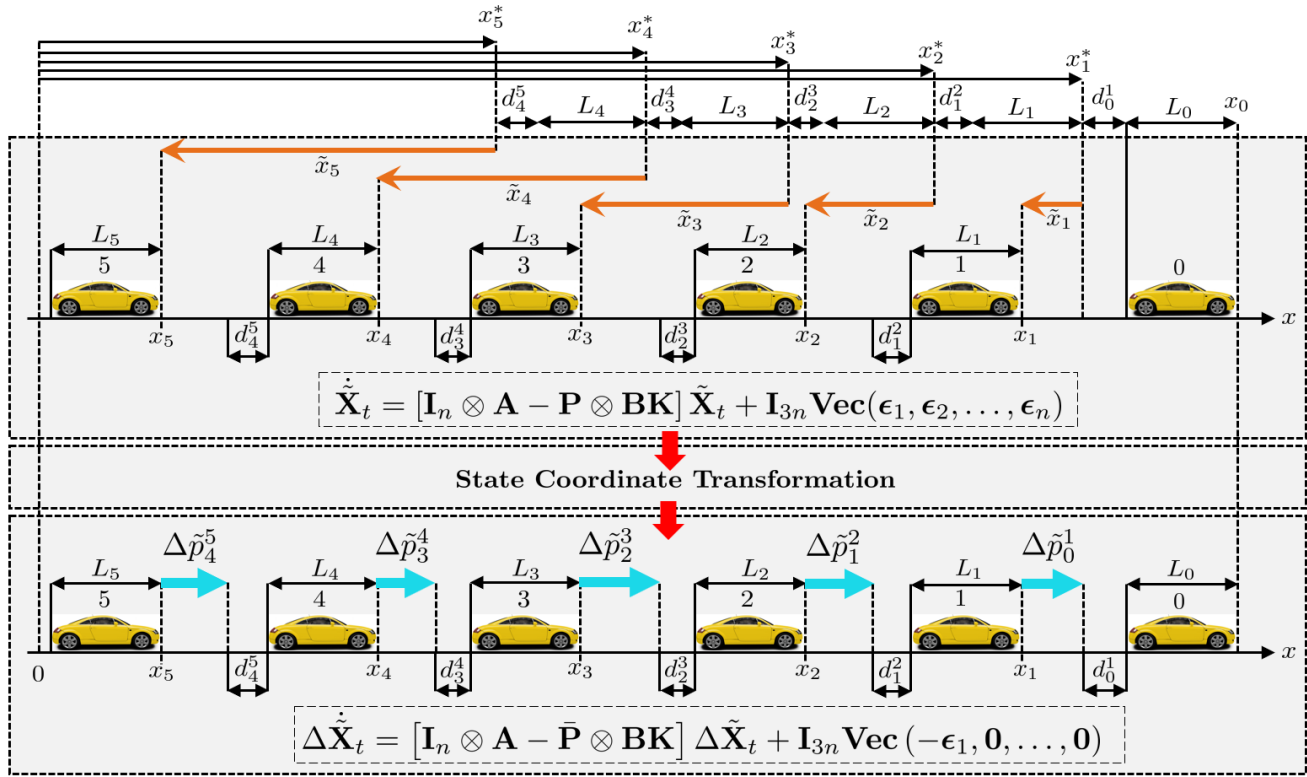


Fig. 7: Illustration of platoon dynamics with ‘follower-leader’ and neighboring ‘follower-predecessor’ state errors.

$(\cup_{j \in \beta_i} \cup_{\kappa=i+1}^{j-1} \zeta_\kappa)$  in which the set  $\zeta_\kappa$  is defined as  $\zeta_\kappa \triangleq \{(\kappa, \kappa+1)\}$ . Note that the sets  $\alpha_i$  and  $\beta_i$  are not empty sets at the same time. For  $i=0, \dots, n-1$ , assuming  $\Delta \tilde{v}_i^{i+1}(0) = \Delta \tilde{u}_i^{i+1}(0) = 0$ , and all initial TIDEs are equal to  $\mu$ , i.e.,  $\Delta \tilde{p}_i^{i+1}(0) = \mu$ , in Laplacian domain we have

$$\Delta \tilde{X}_i^{i+1}(s) = \mathbf{T}_1 \Delta \tilde{p}_i^{i+1}(s) - \mathbf{T}_2 \mu \quad (37)$$

where  $\mathbf{T}_1 \triangleq [1; s; s^2]$  and  $\mathbf{T}_2 \triangleq [0; 1; s]$ . Given (30),  $\Delta \tilde{p}_i^{i+1}(s)$ , for  $i=0, \dots, n-1$ , would be the summation of zero-state ( $\Delta \tilde{X}_i^{i+1}(0) = 0$ ) response and zero-input ( $\Delta \tilde{u}_i^{i+1} = 0$ ) response.

**Theorem 3:** Given (15), (30), and (37), TIDE between neighboring vehicles would be according to

$$\begin{aligned} \Delta \tilde{p}_i^{i+1}(s) = & \Psi_i(s) + H_i(s) \sum_{j \in \alpha_i} \sum_{\kappa=j}^{i-1} \Delta \tilde{p}_\kappa^{\kappa+1}(s) \\ & + H_i(s) \sum_{j \in \beta_i} \sum_{\kappa=i+1}^{j-1} \Delta \tilde{p}_\kappa^{\kappa+1}(s) + \frac{U(0.5-i)(1+\tau s)a_0(s)}{\tau(\tau s^3 + (1+h)s^2 + bs + k)} \end{aligned} \quad (38)$$

where

$$H_i(s) = \frac{\frac{h}{\tau}s^2 + \frac{b}{\tau}s + \frac{k}{\tau}}{s^3 + \bar{h}_i s^2 + \bar{b}_i s + \bar{k}_i}; \quad \alpha_i \neq \emptyset \text{ or } \beta_i \neq \emptyset \quad (39)$$

and

$$\Psi_i(s) = \frac{\mu \left( s^2 + \frac{1 + (|\mathbf{J}_i| - \gamma_i)h}{\tau}s + \frac{(|\mathbf{J}_i| - \gamma_i)b}{\tau} \right)}{s^3 + \bar{h}_i s^2 + \bar{b}_i s + \bar{k}_i}; \quad i=0, \dots, n-1 \quad (40)$$

in which  $\bar{h}_i = \frac{1 + |\mathbf{J}_i|h}{\tau}$ ,  $\bar{b}_i = \frac{|\mathbf{J}_i|b}{\tau}$ ,  $\bar{k}_i = \frac{|\mathbf{J}_i|k}{\tau}$ , and  $\gamma_i = \sum_{j \in \alpha_i} (i-j) + \sum_{j \in \beta_i} (j-i-1)$ .

**Proof:** Given (30), the zero-input response, let be defined as  $\Delta \tilde{p}_{i,zi}^{i+1}(s)$ , would be according to

$$\Delta \tilde{p}_{i,zi}^{i+1}(s) = \mathbf{C}_i^{i+1} (s\mathbf{I}_3 - \mathbf{A}_i^{i+1})^{-1} \Delta \tilde{X}_i^{i+1}(0) = \frac{\mu(s^2 + \bar{h}_i s + \bar{b}_i)}{s^3 + \bar{h}_i s^2 + \bar{b}_i s + \bar{k}_i} \quad (41)$$

where  $\mathbf{I}_3$  is the identity matrix of size 3. Also, the zero-state response, let be defined as  $\Delta \tilde{p}_{i,zs}^{i+1}(s)$ , would be

$$\Delta \tilde{p}_{i,zs}^{i+1}(s) = G_i^{i+1}(s) \Delta \tilde{u}_i^{i+1}(s) \quad (42)$$

in which given (32) and (37) we have  $G_i^{i+1}(s) = \mathbf{C}_i^{i+1} (s\mathbf{I}_3 - \mathbf{A}_i^{i+1})^{-1} \mathbf{B}$  and

$$\Delta \tilde{u}_i^{i+1}(s) = \frac{U(0.5-i)(1+\tau s)a_0(s)}{\tau} + \bar{\Delta} \tilde{u}_i^{i+1}(s) \quad (43)$$

where

$$\begin{aligned} \bar{\Delta} \tilde{u}_i^{i+1}(s) = & \mathbf{K} \mathbf{T}_1 \sum_{j \in \alpha_i} \sum_{\kappa=j}^{i-1} \Delta \tilde{p}_\kappa^{\kappa+1}(s) - \mathbf{K} \mathbf{T}_2 \sum_{j \in \alpha_i} \sum_{\kappa=j}^{i-1} \mu \\ & + \mathbf{K} \mathbf{T}_1 \sum_{j \in \beta_i} \sum_{\kappa=i+1}^{j-1} \Delta \tilde{p}_\kappa^{\kappa+1}(s) - \mathbf{K} \mathbf{T}_2 \sum_{j \in \beta_i} \sum_{\kappa=i+1}^{j-1} \mu \end{aligned} \quad (44)$$

Thus  $G_i^{i+1}(s) = \frac{1}{\tau} (s^3 + \bar{h}_i s^2 + \bar{b}_i s + \bar{k}_i)^{-1}$  and simplifying (44)

results in

$$\begin{aligned} \bar{\Delta} \tilde{u}_i^{i+1}(s) &= (hs^2 + bs + k) \\ &\times \left( \sum_{j \in \alpha_i, \kappa=j}^{i-1} \sum \Delta \tilde{p}_\kappa^{i+1}(s) + \sum_{j \in \beta_i, \kappa=i+1}^{j-1} \sum \Delta \tilde{p}_\kappa^{i+1}(s) \right) \\ &- (hs + b) \left( \sum_{j \in \alpha_i, \kappa=j}^{i-1} \sum \mu + \sum_{j \in \beta_i, \kappa=i+1}^{j-1} \sum \mu \right) \end{aligned} \quad (45)$$

using which and substituting  $\Delta \tilde{u}_i^{i+1}(s)$ , (43), into (42) yields

$$\begin{aligned} \Delta \tilde{p}_{i,zs}^{i+1}(s) &= \frac{U(0.5-i)(1+\tau s)a_0(s)}{\tau(\tau s^3 + (1+h)s^2 + bs + k)} + \frac{\frac{h}{\tau}s^2 + \frac{b}{\tau}s + \frac{k}{\tau}}{s^3 + \bar{h}_i s^2 + \bar{b}_i s + \bar{k}_i} \\ &\times \left( \sum_{j \in \alpha_i, \kappa=j}^{i-1} \sum \Delta \tilde{p}_\kappa^{i+1}(s) + \sum_{j \in \beta_i, \kappa=i+1}^{j-1} \sum \Delta \tilde{p}_\kappa^{i+1}(s) \right) \\ &\frac{\mu \left( \sum_{j \in \alpha_i} (i-j) + \sum_{j \in \beta_i} (j-i-1) \right) \left( \frac{h}{\tau}s + \frac{b}{\tau} \right)}{s^3 + \bar{h}_i s^2 + \bar{b}_i s + \bar{k}_i} \end{aligned} \quad (46)$$

Therefore, given (41) and (46) we have  $\Delta \tilde{p}_i^{i+1}(s) = \Delta \tilde{p}_{i,zs}^{i+1}(s) + \Delta \tilde{p}_{i,zs}^{i+1}(s)$  which is equal to (38). Therefore, the proof completed. ■

#### A. Mapping Between TIDEs and Initial Conditions

Calculating (38) for  $i=0, \dots, n-1$  and stacking them together, after some mathematical manipulation, it is possible to reformulate (38) in the following compact form:

$$\Delta \tilde{\mathbb{P}}(s) = \mathbf{Q}^{-1}(s) (\Psi(s) + \mathbb{U}(s)) \quad (47)$$

such that  $\Delta \tilde{\mathbb{P}}(s) \triangleq [\Delta \tilde{p}_0^1(s); \Delta \tilde{p}_1^2(s); \dots; \Delta \tilde{p}_{n-1}^n(s)]$ ,  $\Psi(s) \triangleq [\Psi_0(s); \Psi_1(s); \dots; \Psi_{n-1}(s)]$ , and  $\mathbf{Q}(s) \in \mathbb{C}^{n \times n}$  whose elements are defined as

$$q_{ij}(s) = \begin{cases} 1 & \text{if } i=j \\ \bar{p}_{ij} H_{i-1}(s) & \text{if } i \neq j \end{cases} \quad (48)$$

where  $\bar{p}_{ij}$  are defined in (34). Also,  $\mathbb{U}(s) \in \mathbb{C}^{n \times 1}$  such that  $\mathbb{U}(s) \triangleq [\frac{(1+\tau s)a_0(s)}{\tau(\tau s^3 + (1+h)s^2 + bs + k)}; 0; \dots; 0]$ . Therefore, if we define the elements of  $\mathbf{Q}^{-1}(s)$  as  $Q_{(i+1)j}^{-1}(s)$ , then exploring (47) yields

$$\begin{aligned} \Delta \tilde{p}_i^{i+1}(s) &= \sum_{j=1}^n Q_{(i+1)j}^{-1}(s) \Psi_{j-1}(s) \\ &+ \frac{U(0.5-i)Q_{11}^{-1}(s)(1+\tau s)a_0(s)}{\tau(\tau s^3 + (1+h)s^2 + bs + k)} \end{aligned} \quad (49)$$

#### B. Different Scenarios for TIDEs

Given (49), it follows that  $\Delta \tilde{p}_i^{i+1}(t)$  represents the impulse response of  $\Delta \tilde{p}_i^{i+1}(s)$ , or equivalently the inverse Laplace transform of  $\Delta \tilde{p}_i^{i+1}(s)$ . Consequently, for a given  $\mathbf{K} = [k, b, h]$ , the appropriate control gains necessary to ensure safe and collision-free distances can be determined based on the relationship between TIDEs, safe and desired IDs. The different scenario are illustrated in Fig. 8. If  $\Delta \tilde{p}_i^{i+1}(t) > -(d_i^{i+1} - d_{i,i+1}^s)$

holds during the travel time (TT), it leads to a stable-safe distance over TT (cases **a** and **b**). Similarly, when  $\Delta \tilde{p}_i^{i+1}(t) > -d_i^{i+1}$  holds within the TT, and  $\Delta \tilde{p}_i^{i+1}(t) < -(d_i^{i+1} - d_{i,i+1}^s)$  occurs during TT, it results in a stable-unsafe distance over TT (case **c**). Conversely, if  $\Delta \tilde{p}_i^{i+1}(t) \leq -d_i^{i+1}$  takes place over the TT, it leads to a stable-collision occurrence within platoon (case **d**). Note that, in Fig. 8,  $D_i^{i+1}(t) = x_i(t) - x_{i+1}(t) - L_i = \Delta \tilde{p}_i^{i+1}(t) + d_i^{i+1}$  exhibits the real distance between neighboring vehicles  $i$  and  $i+1$ . Please observe that when  $\Delta \tilde{p}_i^{i+1}(t)$  converges to zero, signifying a stable platoon, the actual distance between adjacent vehicles will also converge to the desired values.

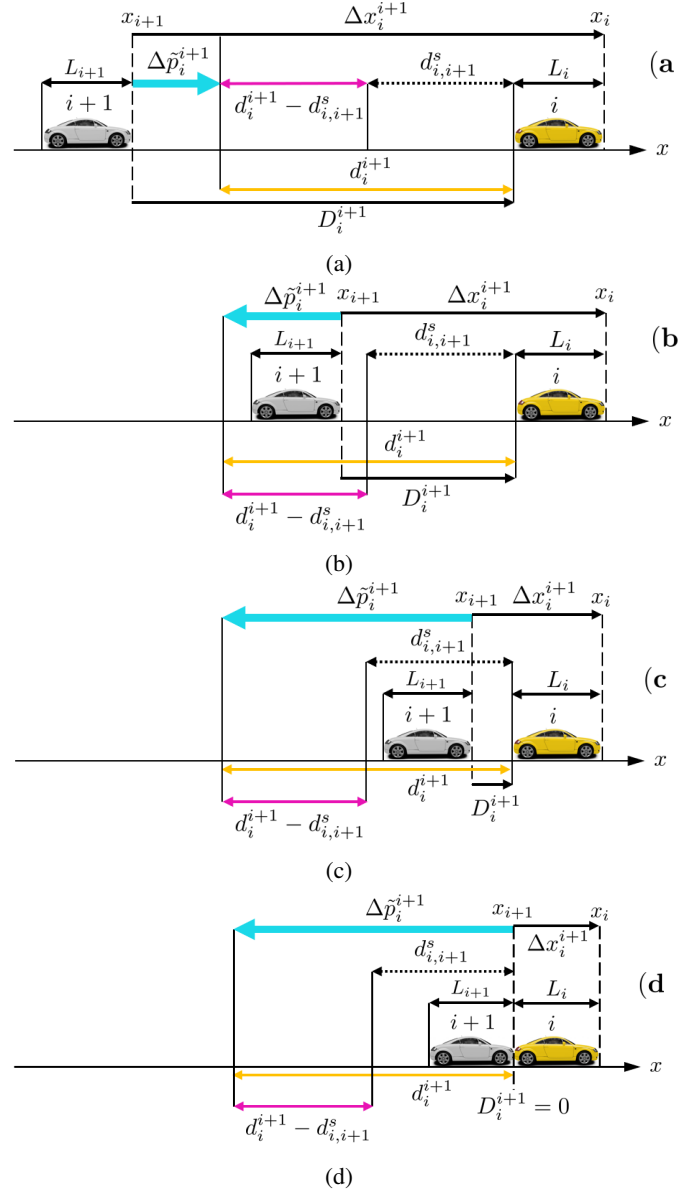


Fig. 8: Portraying different situations featuring transient inter-vehicle distance errors (TIDEs) among neighboring vehicles.

## VII. SIMULATIONS AND RESULTS

In this section, we present simulation results that serve to validate the theoretical findings. To do so, we consider

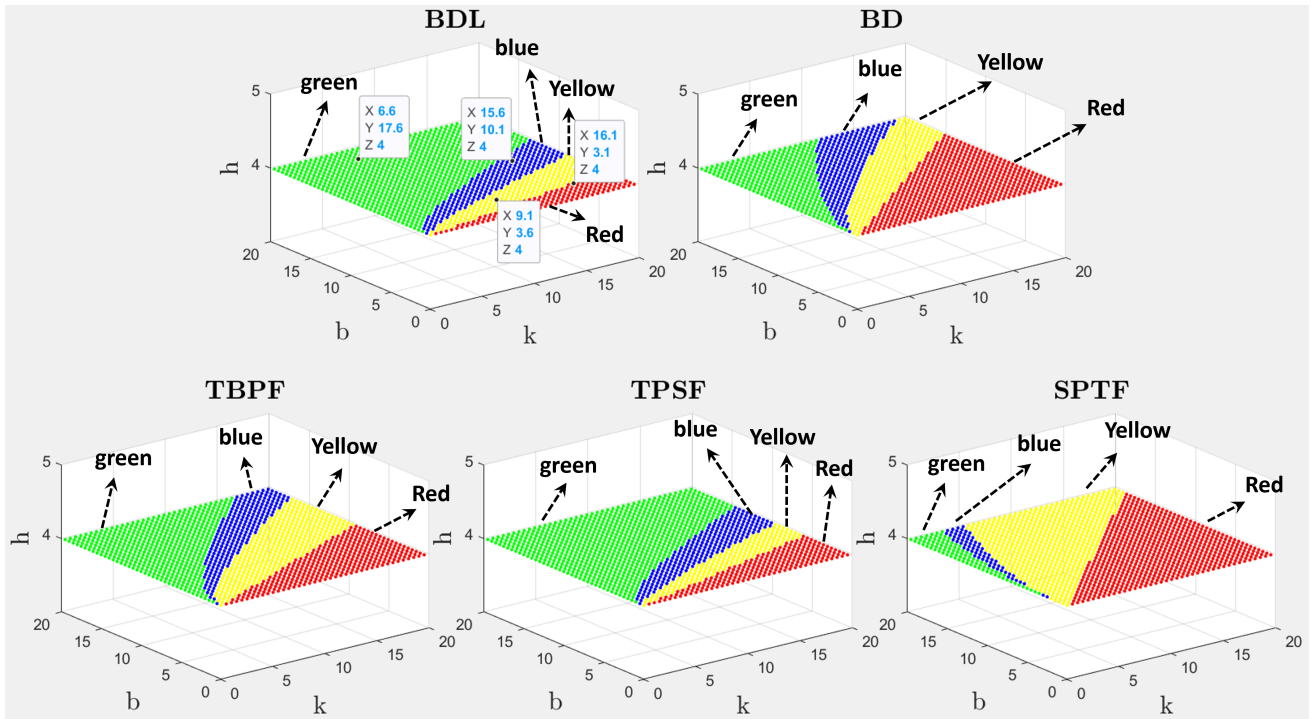


Fig. 9: Control Gain Categories: Unstable (red), Stable-Collision (yellow), Stable-Unsafe (blue), and Stable-Safe (green). Desired and safe distances between neighboring vehicles:  $5m$  and  $3m$ , respectively.

a platoon comprising one leader and five followers, with a constant distance policy set at  $5m$ . Within the simulations, all vehicles begin with initial velocities and accelerations set to zero. Their lengths are uniform at  $4m$ . Furthermore, the safe distance between vehicles is set at  $3m$ , denoted as  $d_{i,i+1}^s = 3m$ .

#### A. Comparing BDCTs Based on TIDE Performance

In the provided BDCTs (see Fig. 1), stability analysis reveals that BDL, BD, and TBPF topologies exhibit real eigenvalues in their matrices  $\mathbf{P}$  and  $\bar{\mathbf{P}}$  (defined in (9) and (34)), while TPSF and SPTF topologies feature a mix of real and conjugate complex eigenvalues. For simulations, let control gains  $k$  and  $b$  vary between 0.1 and 19.6 (with 0.5 increments). Also, we assume that  $\tau=1$ ,  $h=4$ , and the absolute value of leader's acceleration over travel time is  $8m/s^2$ . Unstable control gains are identified when stability conditions are not met, while stable control gains are those satisfying the conditions.

Further analysis, using (49) and the approach detailed in the 'Different Scenarios for TIDES' subsection of the previous section, reveals which control gains lead to unstable, stable-collision, stable-unsafe, or stable-safe distances between neighboring vehicles. These findings are visually represented in Fig. 9, with red indicating unstable, yellow for stable-collision, blue for stable-unsafe, and green for stable-safe gains. Referring to Fig. 9, several noteworthy conclusions can be made:

- 1) **BDL Reigns Supreme:** BDL topology emerges as the front-runner, boasting larger stable and stable-safe areas, indicating its superior performance in platoon control.
- 2) **Leader Broadcasting:** Broadcasting the leader's state, as demonstrated in the BDL topology, significantly elevates platoon performance compared to the conventional BD topology.
- 3) **SPTF's Limitations:** SPTF displays limitations, with the smallest stable area and the largest stable-collision area, suggesting challenges in maintaining platoon stability.
- 4) **BD vs. SPTF:** Despite SPTF providing more information from vehicles behind, BD outperforms it, highlighting the impact of information sources on performance.
- 5) **TPSF's Advantage:** TPSF outperforms TBPF, even though TBPF offers additional information from vehicles behind, emphasizing the significance of information exchange with vehicles ahead.
- 6) **Information from Rear Impacts Performance:** The introduction of extra information from vehicles behind, beyond the immediate follower, is associated with a degradation in platoon performance.
- 7) **BD, TPSF, SPTF Comparison:** TPSF, with additional information from vehicles ahead, enhances performance compared to BD. Conversely, SPTF, with extra rearward information, diminishes performance.
- 8) **BDL vs. TPSF Parity:** BDL and TPSF exhibit comparable performance levels. However, it appears that performance could further improve if the additional information from vehicles ahead originates from the leader vehicle.

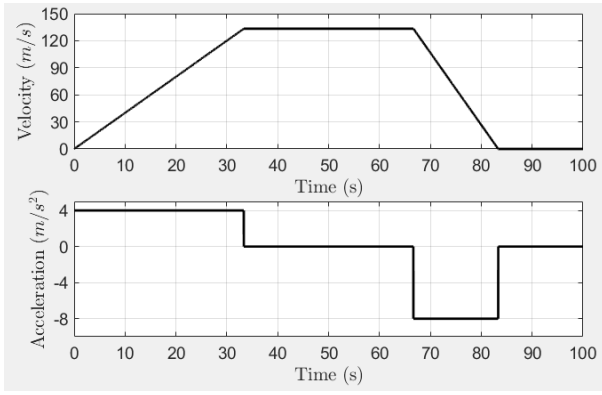


Fig. 10: Leader's velocity and acceleration.

### B. Analysis Validation for TIDE Study

Consider time interval  $t_i^1 \leq t < t_i^2$  during which the leader vehicle's acceleration remains constant at  $a_i^0$ . Therefore, for each time interval we can apply basic physics principles to find its velocity ( $v_i^0$ ) and position ( $x_i^0$ ):

$$\begin{aligned} v_i^0(t) &= a_i^0(t - t_i^1) + v_i^0(t_i^1) \\ x_i^0(t) &= \frac{1}{2}a_i^0(t - t_i^1)^2 + v_i^0(t - t_i^1) + x_i^0(t_i^1) \end{aligned} \quad (50)$$

Fig. 10 depicts an arbitrary acceleration and the associated velocity trajectories we have considered for the leader vehicle for the simulations. Considering (8), and assuming a sampling time of  $\Delta t$ , we can calculate the updated  $\tilde{\mathbf{X}}_i(t + \Delta t)$  as follows:

$$\tilde{\mathbf{X}}_i(t + \Delta t) = \left( \mathbf{I}_{3n} + \tilde{\mathbf{A}}_i \Delta t \right) \tilde{\mathbf{X}}_i(t) + \Delta t \mathbf{Vec}(\epsilon_1, \epsilon_2, \dots, \epsilon_n) \quad (51)$$

Here,  $\mathbf{I}_{3n}$  is the identity matrix of size  $3n$ . Now, Given the acceleration trajectory of leader vehicle, using (3), and noting that  $\tilde{\mathbf{X}}_{i+1}(t) = \mathbf{X}_{i+1}(t) - \mathbf{X}_{i+1}^*(t)$ , other than TIDEs, we can find the follower vehicles' position, velocity and acceleration trajectories. The communication topology is considered to be the BDL topology, and the initial positions are selected as  $x_i(0) = -17 \times i$  m,  $i=0,1,\dots,5$ , where given  $d_i^{i+1} = 5m$ , and  $d_{i,s}^{i+1} = 3m$ , the initial TIDE between neighboring vehicles would be  $\Delta \tilde{p}_i^{i+1}(0) = 8m$ . Additionally, we employ a sampling time of  $0.01s$ . The simulation time is established as  $100s$ , though for the sake of clarity in presentation, results may be shown for time intervals less than  $100s$ .

Associated TIDE trajectories of selected points from the BDL topology (Fig. 9) are illustrated in Fig. 11:

- 1)  $\mathbf{K} = [16.1, 3.1, 4]$  (from the unstable area), error trajectories diverge, rendering the platoon unstable.
- 2)  $\mathbf{K} = [9.1, 3.6, 4]$  (from the stable-collision area) results in converging error trajectories, but some cross the red-dashed line ( $-5m$  error), indicating collisions.
- 3)  $\mathbf{K} = [15.6, 10.1, 4]$  (from the stable-unsafe area) leads to converging error trajectories, with some crossing the blue-red line ( $-2m$  error), signifying violations of the safe distance.
- 4)  $\mathbf{K} = [6.6, 17.6, 4]$  (from the stable-safe area) results in converging trajectories that do not cross the red-dashed

(collision) or blue-dashed (safe distance) lines, ensuring the maintenance of a safe distance between vehicles.

Therefore, the error trajectories validate the identified unstable, stable-collision, stable-unsafe, and stable-safe areas from the provided analysis elaborated on in Section VII.

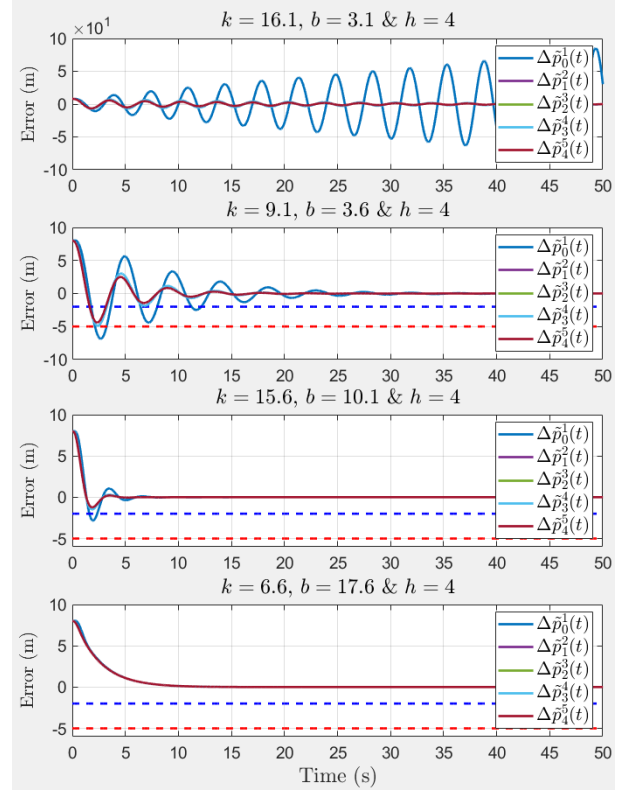


Fig. 11:  $\Delta \tilde{p}_i^{i+1}(t)$  trajectories of selected points from the BDL topology (see Fig. 9).

### C. Tracking Performance

Platooning aims to achieve two vital objectives: 1) aligning followers with the leader's velocity and acceleration, and 2) ensuring IDs converge to preset values, assumed here to be  $5m$ . In our demonstration within the BDL topology, we have chosen representative  $\mathbf{K}$  points from each stability region (see Fig. 9). Fig. 12 displays position, velocity, and acceleration trajectories for  $i=1,\dots,5$  at these selected points. Within stable regions (yellow, blue, and green areas), we observe velocities and accelerations converging to match the leader's values. The convergence times vary among points, with the stable-safe point showing the quickest convergence and the stable-collision point the slowest.

In line with our explanation in the 'Different Scenarios for TIDEs' section, selected points within stable regions demonstrate error convergence to zero, ensuring attainment of the predefined desired distances between neighboring vehicles.

### D. High-Fidelity Simulation of Truck Platooning

We have assessed the controller's performance and communication topologies in realistic vehicle platooning using

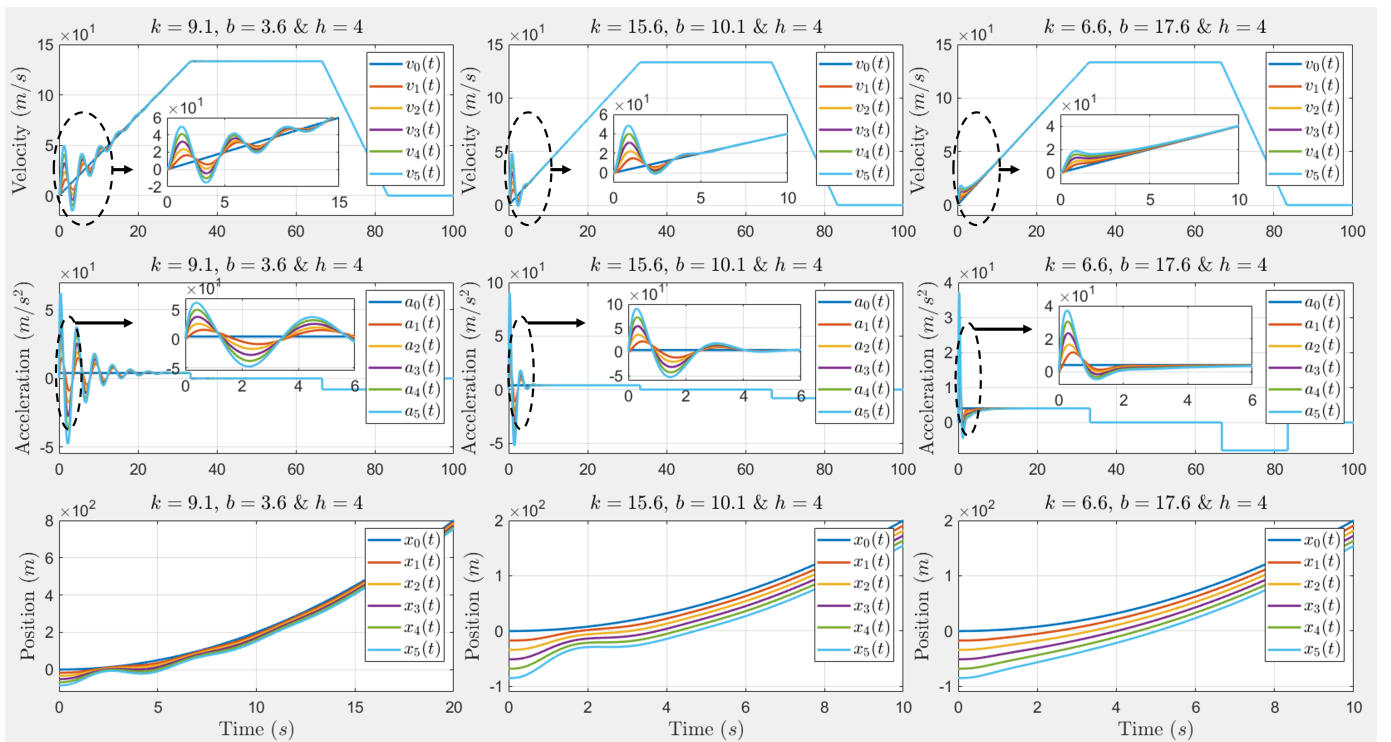


Fig. 12: Velocity, acceleration and position trajectories for BDL topology under control gains  $\mathbf{K}=[9.1,3.6,4]$  (stable-collision),  $\mathbf{K}=[15.6,10.1,4]$  (stable-unsafe) and  $\mathbf{K}=[6.6,17.6,4]$  (stable-safe), respectively.

MATLAB's Vehicle Dynamics Blockset for simulation, employing both BDL and BD communications. Each vehicle's dynamics in the platooning setup encompassed key aspects, including vehicle geometry, suspension, tire, powertrain, and steering/braking systems. The platooning controller governed desired acceleration input for each vehicle, maintaining a fixed steering angle of zero degrees, focusing on longitudinal control.

In addition to the intricate components of vehicle dynamics modeling, the platooning scenario also integrates vehicle-to-vehicle (V2V) communication for deployment. In the realm of communication modeling, each vehicle within the platoon is equipped with V2V transmitters and receivers. Specifically, we configure the communication model to utilize BDL and BD communication protocols. The transmitters are responsible for transmitting basic safety messages (BSMs) containing pose information, while the receivers within the platoon's followers intercept and extract this valuable data from the BSMs. Subsequently, the information obtained by the receivers of the platoon followers is employed by their respective controllers to compute the necessary acceleration for maintaining the desired following distance from the lead vehicle and effectively tracking its movements.

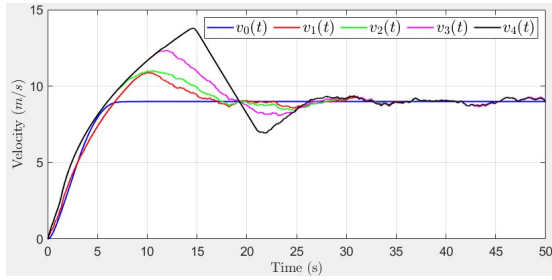
The platooning setup includes one leader and four followers. Each follower has a platooning controller (specified in (4)) that regulates longitudinal controls to maintain a constant spacing from the preceding vehicle while following the lead vehicle. The inbuilt vehicle dynamics are modeled using a six degrees of freedom tractor-trailer system, representing a three-axle tractor towing a three-axle trailer through a hitch. Both the tractor and trailer have individual models for their

vehicle body, wheels, and suspension. The vehicle lengths are set at  $17.2m$ , and the safe and desired intervehicle spacing are established at  $7m$  and  $3m$ . Identical control gains are applied to each follower vehicle, defined as  $\mathbf{K}=[20,25,4]$ . Additionally, the initial positions for the trucks are initialized as  $x_i(0)=-32 \times i$  for  $i=0$  to  $4$ .

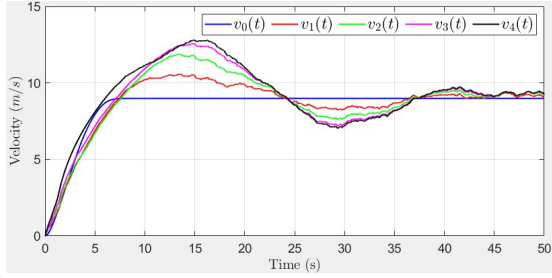
Figs. 13a and 13b illustrate the vehicle velocities under BDL and BD topologies. This simulation emphasizes the substantial enhancement in velocity tracking for follower vehicles achieved through the broadcast of the leader vehicle's state. Additionally, in Figs. 14a and 14b, the desired and safe distances between vehicles, as well as the actual distances between adjacent vehicles in the platoon, are presented. This simulation outcome further underscores the improved platoon performance in coordinating vehicles with the desired intervehicle distances, resulting from the broadcast of the leader vehicle's state. It is noteworthy that in the BDL topology, the distances between vehicles consistently remain above the safe distance threshold, while in the BD topology, the distance between the leader and the first follower has breached the safe distance threshold. Fig. 15 shows the corresponding truck platooning at times  $t=0s$  and  $t=50s$ . Please note that an associated simulation video accompanies these results as pointed out to in Fig. 15.

## VIII. CONCLUSION

While guaranteeing internal stability is essential for achieving desirable steady-state performance, it cannot ensure favorable transient dynamics of intervehicle distances among adjacent vehicles. To address this, we introduced a novel

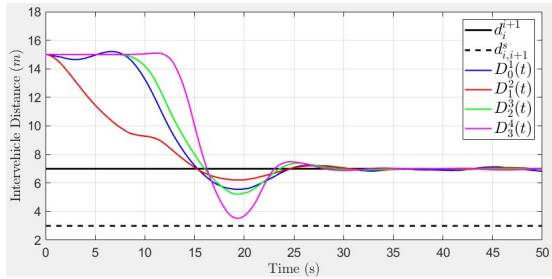


(a) Vehicles' velocities under BDL topology

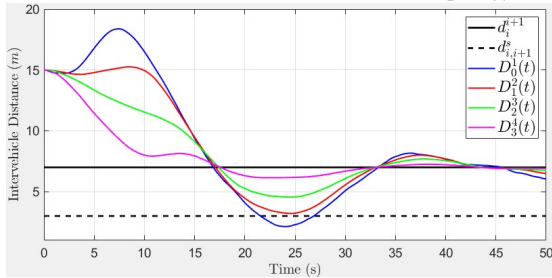


(b) Vehicles' velocities under BD topology

Fig. 13: Illustrating the beneficial impact of broadcasting the state of the leader vehicle to FVs.



(a) Distance between trucks under BDL topology

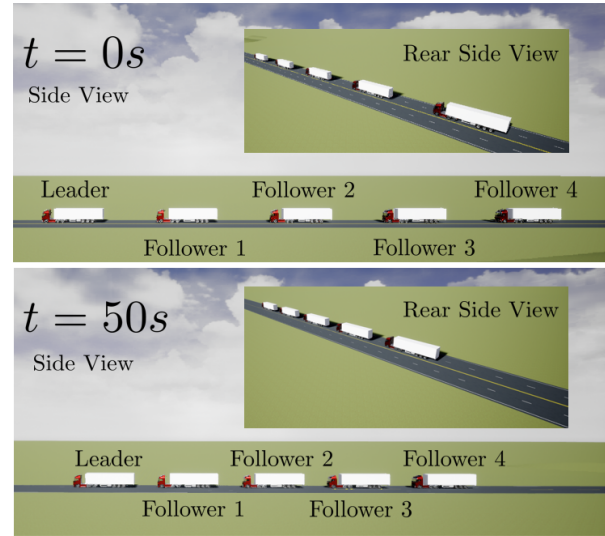


(b) Distance between trucks under BD topology

Fig. 14: Illustrating the beneficial impact of broadcasting the state of the leader vehicle to FVs.

closed-loop distance dynamic model for platoons, shifting our focus from follower-leader state differences to neighboring-vehicle state differences.

Through this innovative dynamic model, we not only assessed system stability but also conducted transient intervehicle distance analysis for adjacent vehicles. Considering the leader vehicle's state, and based on initial conditions, vehicle's engine time constants, the number of vehicles, and communication type, we analytically determined distance trajectories between each pair of neighboring vehicles. Our


 Fig. 15: Truck Platooning under BDL topology. States of platoon at  $t=0s$  and  $t=50s$ . Please check the link <https://youtu.be/rxQ-XsYFaEM?si=uJIToELSiFWvoEH> to watch the simulation video for BDL case.

exploration of various control gains allowed us to investigate how distance trajectories behave across different bidirectional communication topologies (BDCTs).

These investigations highlighted the advantages and disadvantages of different BDCTs. Notably, our findings indicated that within BDCTs and with a given control gain, receiving information from vehicles far behind may adversely impact platoon performance. Conversely, obtaining information from vehicles far ahead can enhance TIDs, ensuring they remain within a safe range. Furthermore, we demonstrated that broadcasting the leader vehicle's state to other vehicles holds the potential to enhance overall platoon performance. Finally, simulations are provided to substantiate the theoretical finding.

## REFERENCES

- [1] A. Alam, B. Besselink, V. Turri, J. Mårtensson, and K. H. Johansson, "Heavy-duty vehicle platooning for sustainable freight transportation: A cooperative method to enhance safety and efficiency," *IEEE Control Systems Magazine*, vol. 35, no. 6, pp. 34–56, 2015.
- [2] C. Bonnet and H. Fritz, "Fuel consumption reduction in a platoon: Experimental results with two electronically coupled trucks at close spacing," SAE Technical Paper, Tech. Rep., 2000.
- [3] S. E. Shladover, D. Su, and X.-Y. Lu, "Impacts of cooperative adaptive cruise control on freeway traffic flow," *Transportation Research Record*, vol. 2324, no. 1, pp. 63–70, 2012.
- [4] F.-Y. Wang, "Parallel control and management for intelligent transportation systems: Concepts, architectures, and applications," *IEEE Transactions on Intelligent Transportation Systems*, vol. 11, no. 3, pp. 630–638, 2010.
- [5] J. Zhou and H. Peng, "Range policy of adaptive cruise control vehicles for improved flow stability and string stability," *IEEE Transactions on intelligent transportation systems*, vol. 6, no. 2, pp. 229–237, 2005.
- [6] G. Orosz, "Connected cruise control: modelling, delay effects, and nonlinear behaviour," *Vehicle System Dynamics*, vol. 54, no. 8, pp. 1147–1176, 2016.
- [7] B. Besselink and K. H. Johansson, "String stability and a delay-based spacing policy for vehicle platoons subject to disturbances," *IEEE Transactions on Automatic Control*, vol. 62, no. 9, pp. 4376–4391, 2017.

- [8] P. A. Ioannou and C.-C. Chien, "Autonomous intelligent cruise control," *IEEE Transactions on Vehicular Technology*, vol. 42, no. 4, pp. 657–672, 1993.
- [9] D. Swaroop and J. K. Hedrick, "Constant spacing strategies for platooning in automated highway systems," 1999.
- [10] S. S. Stankovic, M. J. Stanojevic, and D. D. Siljak, "Decentralized overlapping control of a platoon of vehicles," *IEEE Transactions on Control Systems Technology*, vol. 8, no. 5, pp. 816–832, 2000.
- [11] P. Seiler, A. Pant, and K. Hedrick, "Disturbance propagation in vehicle strings," *IEEE Transactions on automatic control*, vol. 49, no. 10, pp. 1835–1842, 2004.
- [12] Y. Zheng, S. E. Li, J. Wang, D. Cao, and K. Li, "Stability and scalability of homogeneous vehicular platoon: Study on the influence of information flow topologies," *IEEE Transactions on intelligent transportation systems*, vol. 17, no. 1, pp. 14–26, 2015.
- [13] A. Ghasemi, R. Kazemi, and S. Azadi, "Stable decentralized control of a platoon of vehicles with heterogeneous information feedback," *IEEE Transactions on Vehicular Technology*, vol. 62, no. 9, pp. 4299–4308, 2013.
- [14] S. E. Li, X. Qin, Y. Zheng, J. Wang, K. Li, and H. Zhang, "Distributed platoon control under topologies with complex eigenvalues: Stability analysis and controller synthesis," *IEEE Transactions on Control Systems Technology*, vol. 27, no. 1, pp. 206–220, 2017.
- [15] M. Pirani, S. Baldi, and K. H. Johansson, "Impact of network topology on the resilience of vehicle platoons," *IEEE Transactions on Intelligent Transportation Systems*, 2022.
- [16] T. Ruan, H. Wang, L. Zhou, Y. Zhang, C. Dong, and Z. Zuo, "Impacts of information flow topology on traffic dynamics of cav-mv heterogeneous flow," *IEEE Transactions on Intelligent Transportation Systems*, 2022.
- [17] C. K. Verginis, C. P. Bechlioulis, D. V. Dimarogonas, and K. J. Kyriakopoulos, "Robust distributed control protocols for large vehicular platoons with prescribed transient and steady-state performance," *IEEE Transactions on Control Systems Technology*, vol. 26, no. 1, pp. 299–304, 2017.
- [18] Y. Zheng, S. E. Li, K. Li, and L.-Y. Wang, "Stability margin improvement of vehicular platoon considering undirected topology and asymmetric control," *IEEE Transactions on Control Systems Technology*, vol. 24, no. 4, pp. 1253–1265, 2015.
- [19] A. Liu, T. Li, Y. Gu, and H. Dai, "Cooperative extended state observer based control of vehicle platoons with arbitrarily small time headway," *Automatica*, vol. 129, p. 109678, 2021.
- [20] X. Ge, S. Xiao, Q.-L. Han, X.-M. Zhang, and D. Ding, "Dynamic event-triggered scheduling and platooning control co-design for automated vehicles over vehicular ad-hoc networks," *IEEE/CAA Journal of Automatica Sinica*, vol. 9, no. 1, pp. 31–46, 2021.
- [21] X. Ge, Q.-L. Han, J. Wang, and X.-M. Zhang, "Scalable and resilient platooning control of cooperative automated vehicles," *IEEE Transactions on Vehicular Technology*, vol. 71, no. 4, pp. 3595–3608, 2022.
- [22] J. Lan, D. Zhao, and D. Tian, "Data-driven robust predictive control for mixed vehicle platoons using noisy measurement," *IEEE Transactions on Intelligent Transportation Systems*, 2021.
- [23] D. Huang, S. Li, Z. Zhang, Y. Liu, and B. Mi, "Design and analysis of longitudinal controller for the platoon with time-varying delay," *IEEE Transactions on Intelligent Transportation Systems*, 2022.
- [24] G. Yu, P. K. Wong, W. Huang, J. Zhao, X.-B. Wang, and Z.-X. Yang, "Distributed adaptive consensus protocol for connected vehicle platoon with heterogeneous time-varying delays and switching topologies," *IEEE Transactions on Intelligent Transportation Systems*, 2022.
- [25] S. Wen and G. Guo, "Sampled-data control for connected vehicles with markovian switching topologies and communication delay," *IEEE Transactions on Intelligent Transportation Systems*, vol. 21, no. 7, pp. 2930–2942, 2019.
- [26] A. Zakerimanesh, T. Qiu, and M. Tavakoli, "Heterogeneous vehicular platooning with stable decentralized linear feedback control," in *2021 IEEE International Conference on Autonomous Systems (ICAS)*. IEEE, 2021, pp. 1–5.



**Amir Zakerimanesh** (Graduate Student Member, IEEE) was born in Tabriz, Iran. He received his B.Sc. and M.Sc. degrees in electrical engineering (control-system) from the Faculty of Electrical and Computer Engineering, University of Tabriz, Tabriz, Iran, in 2012 and 2015, respectively. He is currently pursuing the Ph.D. degree in electrical engineering with the University of Alberta, Edmonton, AB, Canada. His research interests include control theory, machine learning, robotics, computer vision, and intelligent transportation systems.



**Tony Z. Qiu** (Member, IEEE) received the B.Sc. and M.Sc. degrees from Tsinghua University, China, in 2001 and 2003, respectively, and the Ph.D. degree from the University of Wisconsin-Madison in 2007. Since joining the University of Alberta (U of A) in 2009, he founded the Intelligent Transportation Systems (ITS) Research Laboratory, now called the Centre for Smart Transportation (CST). He is also the Scientific Director of the Autonomous Systems Initiative (ASI), a multi-million dollar Campus Alberta Research Program focused on developing artificial intelligence and automated systems. From 2008 to 2009, he worked as a Post-Doctoral Researcher with California PATH Program at the University of California at Berkeley, Berkeley. He is currently a Professor with the Department of Civil and Environmental Engineering, U of A, and holds both the Canada Research Chair in Cooperative Transportation Systems and the NSERC Industrial Research Chair in Intelligent Transportation Systems positions. Through his leadership of the CST, he is working to foster Canadian competitiveness in connected vehicle (CV) technology and research by developing Canada's first CV testbed, ACTIVE-AURORA, a network of six on-road and in-lab testbeds equipped and linked with CV technology. ACTIVE-AURORA provides an ITS and CV testing ground and a multi-institutional collaboration platform. In addition to having completed over 41 research projects totaling more than 6,000,000 in funding, he has published over 160 journals and conference papers, several of which have been chosen for best paper awards. His research focuses on developing analytical models to evaluate and optimize large and complex ITS networks and develop support tools for the agencies that manage these systems. Dr. Qiu has received the 2013 Minister's Award of Excellence in Process Innovation, the 2015 Faculty of Engineering Research Award from the University of Alberta, an award at the 2016 ITS Canada Annual Conference for research collaboration with the City of Edmonton, and the Young ITS Canada Leadership Award for his contributions to the advancement of intelligent transportation systems in June 2019.



**Mahdi Tavakoli** (Senior Member, IEEE) is professor of Electrical and Computer Engineering and Senior University of Alberta Engineering Research Chair in Healthcare Robotics. He received his BSc and MSc degrees in Electrical Engineering from Ferdowsi University and K.N. Toosi University, Iran, in 1996 and 1999, respectively. He received his PhD degree in Electrical and Computer Engineering from the University of Western Ontario, Canada, in 2005. In 2006, he was a post-doctoral researcher at Canadian Surgical Technologies and Advanced

Robotics (CSTAR), Canada. In 2007–2008, he was an NSERC Post-Doctoral Fellow at Harvard University, USA. Dr. Tavakoli's research interests broadly involve the areas of robotics and systems control. Specifically, his research focuses on haptics and teleoperation control, medical robotics, and image-guided surgery. Dr. Tavakoli is the lead author of *Haptics for Teleoperated Surgical Robotic Systems* (World Scientific, 2008). He is a Senior Member of IEEE, Specialty Chief Editor for *Frontiers in Robotics and AI* (Robot Design Section), and an Associate Editor for the *International Journal of Robotics Research*, *IEEE Transactions on Medical Robotics and Bionics*, *IEEE Robotics and Automation Letters*, *IEEE TMECH/AIM Emerging Topics Focused Section*, and *Journal of Medical Robotics Research*.